Comparative Analysis of two Non-Newtonian Fluid Models for a Stretching Cylinder

By

Fatima Munazza

Supervisor

Dr. Muhammad Asif Farooq

Department of Mathematics,

School of Natural Sciences (SNS)

National University of Sciences and Technology (NUST)

Islamabad, Pakistan

2023

THESIS ACCEPTANCE CERTIFICATE

Certified that final copy of MS thesis written by **Fatima Munazza,** (Registration No. **00000365253**), of **School of Natural Sciences** has been vetted by undersigned, found complete in all respects as per NUST statutes/regulations, is free of plagiarism, errors, and mistakes and is accepted as partial fulfillment for award of MS/M.Phil degree. It is further certified that necessary amendments as pointed out by GEC members and external examiner of the scholar have also been incorporated in the said thesis.

Signature: _____

Name of Supervisor: Dr. Muhammad Asif Farooq

Date: _____28-08-2023_____

Signature (HoD): _____

Date: _____29/08/2023_____

Signature (Dean/Principal): _____

Date: ___30.08.2023___

National University of Sciences & Technology

MS THESIS WORK

We hereby recommend that the dissertation prepared under our supervision by: <u>Fatima Munazza,</u> Regn No. <u>00000365253</u> Titled: <u>Comparative Analysis of two Non-Newtonian Fluid Models for Stretching Cylinder</u> be accepted in partial fulfillment of the requirements for the award of **MS** degree.

Examination Committee Members

1. Name: <u>PROF. MERAJ MUSTAFA HASHMI</u>   Signature: _____

2. Name: <u>PROF. MUJEEB UR REHMAN</u>   Signature: _____

Supervisor's Name <u>DR. M. ASIF FAROOQ</u>   Signature: _____

_____
Head of Department

29/08/2023
Date

COUNTERSINGED

Date: 30·08·2023

Dean/Principal

This thesis is dedicated to **my beloved parents** and my sister **Dr. Farhat Jabeen**

Acknowledgment

I would like to begin by expressing my sincere gratitude to **Allah the Almighty**, the Most Gracious, and the Most Merciful for His blessings bestowed upon me during my academic journey and in completing my thesis. May Allah's blessings be upon His final Prophet Muhammad (Peace Be Upon Him), his family and his companions.

I would also like to extend my heartfelt appreciation to my supervisor, Dr. M. Asif Farooq, for his unwavering patience, guidance and support. I have greatly benefited from his wealth of knowledge and meticulous editing. His insightful feedback has challenged me to sharpen my thinking and elevate my work to a higher level. I would also like to express my gratitude and sincere thanks to GEC members, Dr. Meraj Mustafa Hashmi and Dr. Mujeeb ur Rehman for their invaluable assistance.

I am deeply grateful to my parents whose constant love and support have kept me motivated and confident throughout my academic journey. My accomplishments and success are a testament to their unwavering belief in me. My heartfelt thanks go out to my siblings who have kept me grounded, reminded me of what is truly important in life and have always been supportive of my endeavors. Finally, I owe a debt of gratitude to my beloved friends for their invaluable suggestions, support and motivation.

Abstract

The aim of the thesis is to demonstrate comparative analysis of two non-Newtonian fluid models such as Cross viscosity model and Carreau viscosity model. These models are significant for both low and high shear rate regions. The problem of only Cross viscosity model is established to examine heat source in unsteady, MHD nanofluid flow subject to convective boundary conditions past a stretching cylinder incorporated with variable thermal properties. A mathematical model for comparison of both fluids with constant thermal properties are employed for analysis. In transforming governing partial differential equations into ordinary differential equations, similarity variables are utilized that possesses a non-similar solution. The numerical solutions are found utilizing MATLAB package *bvp4c*. The velocity, temperature and concentration curves for various parameters are plotted graphically. The values for the coefficient of skin friction, heat transfer rate, mass transfer rate and micro-organisms local density for various choices of parameters are correspondingly tabulated. It is found that, in absolute sense Carreau nanofluids experience higher drag force in comparison to Cross nanofluids with effect of rising parameters like magnetic, porosity, Weissenberg, unsteadiness, temperature buoyancy and concentration buoyancy parameter. Moreover, there is smaller gyrotactic micro-organisms local density for Carreau fluids in comparison to Cross fluids.

Contents

List of Figures

List of Tables

Chapter 1

Introduction

1.1 Literature Review

The fluid flowing due to stretching surface has significance in engineering and industrial fields such as plastic and metal industries during extrusion process which comprises hot rolling, wire drawing, spinning of fibers illustrated by Altan et al. [1], Fisher [2] and Tadmor et al. [3]. Wang [4] pioneered the concept of flow over stretching cylinder where he utilized the perturbation method to evaluate third order nonlinear governing system of ODEs and found asymptotic solution for high Reynolds number. Imtiaz et al. [5] modelled the problem of stretching cylinder for convective boundary conditions utilizing HAM. The analysis of heat transfer over stretching cylinder using slip boundary conditions was performed by Pandey and Kumar [6]. Poply et al. [7] studied dual solution of MHD flow and its stability on stretching cylinder using partial slip conditions. Ali et al. [8] undergoes investigation on viscous flow over porous and stretching cylinder having non-uniform radius. For more detail in problems of stretching cylinder, see ref. [9] - [11].

Non-Newtonian fluids have range of implementations in plastic and chemical processing industry as well as in the field of food and materials science. They are commonly used in processes such as rubber sheet manufacturing, food processing, hot rolling for paper production, plastic polymer development, optical fiber production, and cosmetic formulation, among others. These fluids are composed of multiple components having complex chemical structures and display varying degrees of elasticity, thixotropy, and shear-dependent viscosity [12]. Consequently, understanding the behavior of non-Newtonian fluids has become a major area of interest for researchers and industry professionals alike.

Cross rheological model first introduced by Cross [13] is utilized widely since it is not only significant for the low shear rate and high shear rate regions but also for power law regions. Certain

implications of the model includes synthesis for polymeric solution, 0.35% aqueous solution of Xanthan gum, blood, aqueous solutions for polymeric latex sphere and polyacrylamide [14]. Escudier et al. [15] conducted experimental analysis by availing cross equations with Xanthan gum (non-Newtonian fluid). Khan et al. [16] considered radially stretching sheet for investigating heat transfer in axisymmetric flow and deduced that, velocity rises while increasing power law index and decreasing thermal boundary layer. While, Nayak et al. [17] discussed two dimensional MHD Cross fluid flow on exponentially stretching surface. Hina et al. [18] assessed heat transfer effects around circular cylinder resulting diminished velocity boundary layer due to increase in Weissenberg number.

Carreau [19] and Cross [13] introduced correlations for shear-rate data that were applicable to a wide range of shear rates using four-parameter apparent viscosity equations. The power law model represents a generalized form of Newtonian fluids. However, it may not be able to predict the viscosity of fluids with both large and small shear rates accurately. To overcome these limitations, new models such as Carreau and Cross fluids have been developed. These models belong to the class of generalized Newtonian fluids and are capable of providing more accurate predictions of fluid behavior in a wider range of shear rates. Lately, only limited attention has been given to examine momentum transport in the context of Carreau and Cross fluid models. Sochi [20] conducted study for analytical solution of Cross and Carreau fluids flowing in thin slits and circular pipes.

The term nanofluids were first proposed by Choi and Eastman [21] which involves nanoparticles having 1 – 100 nm diameter dispersed in base fluid in order to classify colloids. They have higher stability, admissible viscosity, smooth flow along channels exclusive of clogging. It has applications in engineering such as microelectronics, domestic refrigerators, coolant and fuel cells. Nanofluids helps in enhancing thermal conductivity of fluids. Nanoparticles, base fluids and living microorganisms such as algae and oxytaxis bacteria are collectively termed as bio-nanofluids. The presence of these microorganisms in the fluids leads to phenomenon known as bioconvection, which improves the thermal and mass transport properties of the fluid and stabilizes the nanoparticles Kuznetsov et al. [22]. Buongiorno [23] studied flow of nanofluids in convective transport model while assuming incompressible flow, negligible viscosity, external forces and radiative heat transfer under thermal equilibrium of base fluids and nanoparticles. Numerous possible uses of nanofluids was found by Wakif et al. [24] utilizing comprehensive mathematical modelling. Alshehri et al. [25] scrutinized heat transfer and unsteady convective flow of viscous nanofluid through porous stretching/shrinking surface.

Magnetohydrodynamics in industrial processes is crucial since variation in magnetic field aid in altering flow profile. In petroleum production and metallurgical operations, the investigation of MHD on boundary layer flow is necessary, elaborated by Katagiri [26]. In last few decades, researchers showed a lot of interest in heat transfer and MHD flow over stretching cylinder. Hayat

et al. [27] found that increase in magnetic field results decrease in fluid flow strength whereas, temperature profile rises by scrutinizing the problem of heat transfer and MHD flow.Mishra et al. [28] discussed influence of velocity and thermal slip effects towards a stretching cylinder on MHD nanofluid. The MHD flow of hybrid nanofluid instilled with hollow cylinder while analyzing entropy generation was discussed by Tayebi and Ali [29]. Meanwhile, a lot of scientists are eager to investigate thermal performance taking into account different impacts and shapes, see ref. [30] - [32].

Activation energy can be described as the minimum energy required to initiate a chemical reaction. Generally, the relationship between a chemical reaction and mass transfer is complex. Evaluating this relationship can be done by analyzing the decomposition of chemical reactions and production at varying rates in mass transfer and the working fluid. Arrhenius and colleagues [33] were among the first to suggest the use of the Arrhenius activation energy concept for integrating various biochemical processes. They posited that a minimum temperature is necessary for atoms and molecules within a tubular reactor to engage and initiate a chemical transformation. In base carrier fluids, the presence of activation energy significantly influences nanoparticle distribution. Consequently, the impact of activation energy on water nanofluids with sudden interest has garnered substantial attention. Irfan et al. [34] conducted a study to analyze the flow characteristics of a three-dimensional Carreau nanofluid with activation energy under unsteady conditions. Khan et al. [35] examined the impact of bioconvection and viscous dissipation on micropolar nanofluids in the context of activation energy. Their findings revealed that an increase in the Peclet number resulted in a reduced motility rate.

Numerous applications for the phenomenon of heat transfer under convective boundary conditions involves petroleum processing, nuclear power, gas turbines, thermal energy storage and manufacturing industry (drying material). The efficacious implementations of convective boundary conditions compelled various researchers to reconsider the heat transfer problems. Aziz [36] scrutinized the convective boundary conditions for viscous fluid problem in classic Blasius flow and concluded that, Biot number could be employed to administer thickness of thermal boundary layer. Makinde et al. [37] examined the flow formation on boundary layer using convective boundary conditions. Non-similar solution of Eyring-Powell fluid was found by Ray et al [38] by using homotopy analysis method. Babu et al. [39] illustrated phenomenon of heat transfer under convective boundary conditions for jeffery fluid. The Darcy-Forchheimer nanofluid flow was investigated by Mabood et al. [40] by utilizing carbon nanotubes as nanoparticles and integrating convective boundary conditions.

1.2 Fluid as Continuum

A material composed of continuous matter, we call such system as a continuum. The continuum hypothesis states that since matter is composed of molecules, a small volume can contain a large number of molecules. In continuum studies, we are concerned not with the properties of each molecule at a given moment but with the average properties of a large number of molecules around each point especially in liquids. We therefore assume that matter is continuously distributed throughout an imaginary region, with a large number of molecules present in even the smallest volumes.

1.2.1 Compressible/Incompressible Flow

Compressible flows are those fluids whose density changes significantly with changes in pressure. Gases such as air, oxygen, and nitrogen are generally compressible fluids because their density changes dramatically with pressure and temperature. Mathematically,

$$\frac{d\rho}{dt} \neq 0. \tag{1.1}$$

The flow through which density of the fluid stays constant for every small volume is termed incompressible flow.

$$\frac{d\rho}{dt} = 0. \tag{1.2}$$

Furthermore, fluid flows having Mach number higher than 0.3 are categorized as compressible while, flows with Mach number smaller than 0.3 are termed incompressible.

1.2.2 Steady/Unsteady Flow

Steady-state flow means that the fluid properties at any point during the flow of the fluid do not change with time. Mathematically,

$$\frac{\partial \zeta}{\partial t} = 0. \tag{1.3}$$

An unsteady flow is one in which the properties of the fluid at any point during the flow change over time. Mathematically,

$$\frac{\partial \zeta}{\partial t} \neq 0. \tag{1.4}$$

1.2.3 Newtonian/Non-Newtonian Fluids

Newtonian fluids refer to fluids that conform to Newton's law of viscosity. Their viscosity is constant and does not change with the change of shear rate. This behaviour is encapsulated in following mathematical expression:

$$\tau = \mu \frac{du}{dy}, \tag{1.5}$$

wherein τ symbolizes the shear stress, μ is the dynamic viscosity and $\dfrac{du}{dy}$ is the deformation rate.

In contrast, non-Newtonian fluids do not obey Newton's law of viscosity and their viscosity changes with the shear rate. This relationship can be characterized by the subsequent mathematical expression:

$$\tau = K \left(\frac{du}{dy} \right)^n. \tag{1.6}$$

Here, K is the consistency index and n is the rheological index.

1.2.4 Shear Thickening Fluids

Shear thickening fluids, also known as dilatant fluids increases in viscosity as the rate of applied shear enhances. This indicates when a fluid experiences higher levels of deformation or shear, its resistance to flow increases. Numerically, when flow index n is greater than 1, the fluid is termed shear-thickening.
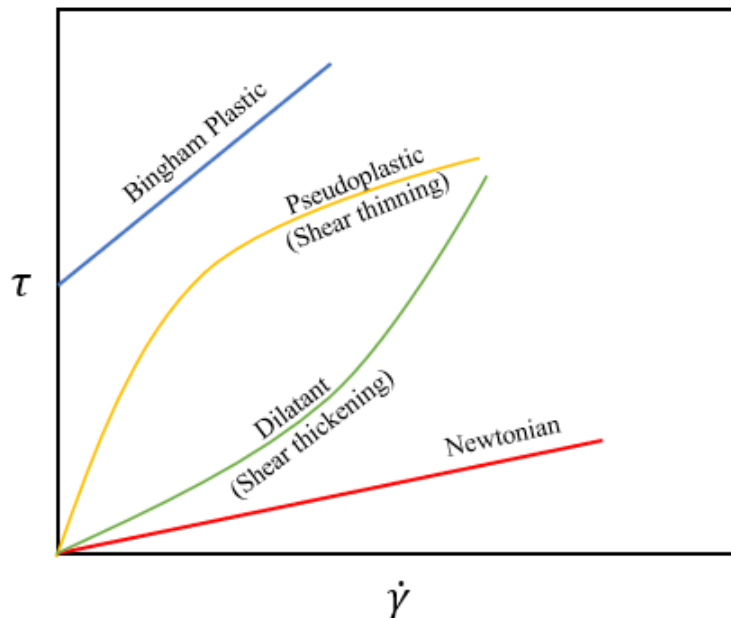
Figure 1.1: Illustration of different types of fluids

1.2.5 Shear Thinning Fluids

Shear-thinning fluids are also known as pseudoplastic fluids, whose viscosity decreases as the rate of applied shear increases. This means when a fluid is subjected to higher levels of deformation, its resistance to flow decreases. Numerically, when flow index follows $0 < n < 1$ then, the fluid is termed shear-thinning.

1.3 Governing Equations

1.3.1 Continuity Equation

The equation of continuity can be defined as the amount of fluid entering into the control volume is same as that of fluid leaving the control volume. Particularly, it is the mass flow rate that remains constant. So, it is basically another form of law of conservation of mass. Here, we can write it as,

$$\frac{\partial \rho}{\partial t} + \overrightarrow{\nabla} \cdot (\rho \overrightarrow{V}) = 0. \tag{1.7}$$

For an incompressible flow, as ρ is constant, the continuity equation becomes,

$$\overrightarrow{\nabla} \cdot \overrightarrow{V} = 0. \tag{1.8}$$

1.3.2 Momentum Equation

The momentum equations are derived from law of conservation of momentum. It can be stated as, the rate at which momentum alters for a fluid in motion equates to the body and surface forces exerted on the fluid. The general momentum equation can be written as,

$$\rho \frac{d\overrightarrow{V}}{dt} = \overrightarrow{\nabla} \cdot \tau + \rho \overrightarrow{g}, \tag{1.9}$$

where, τ, $\overrightarrow{g}$ denotes stress tensor and gravity, respectively and material time derivative is defined as,

$$\frac{d}{dt} = \frac{\partial}{\partial t} + u \frac{\partial}{\partial x} + v \frac{\partial}{\partial y}.$$

1.3.3 Energy Equation

The energy equation has been derived from law of conservation of energy. For a fluid, the energy equation can be written as,

$$\rho c_p \frac{dT}{dt} = \overrightarrow{\nabla} \cdot \left(k \overrightarrow{\nabla} T \right) + \phi, \tag{1.10}$$

where, ρ represents density, c_p denotes specific heat, T is temperature, k is thermal conductivity, ϕ denotes viscous dissipation function defined as

$$\phi = \mu \left[2\left(\frac{\partial u}{\partial x}\right)^2 + 2\left(\frac{\partial v}{\partial y}\right)^2 + 2\left(\frac{\partial w}{\partial z}\right)^2 + \left(\frac{\partial v}{\partial x} + \frac{\partial u}{\partial y}\right)^2 + \left(\frac{\partial w}{\partial y} + \frac{\partial v}{\partial z}\right)^2 + \left(\frac{\partial u}{\partial z} + \frac{\partial w}{\partial x}\right)^2 \right].$$

1.3.4 Concentration Equation

The law of conservation of concentration is illustrated in following mathematical formulation:

$$\frac{dC}{dt} = -\overrightarrow{\nabla} \cdot \overrightarrow{K} + G,$$

where, C, $\overrightarrow{K}$ and G denotes concentration field, diffusion flux and source term due to nuclear, chemical or other factors, respectively. From the Fick's law, we know that diffusion flux is proportional to negative concentration gradient such as,

$$\overrightarrow{K} = -D\overrightarrow{\nabla}C,$$

here, D is proportionality constant termed as diffusivity. Now, the general simplified form of concentration equation will be presented as,

$$\frac{\partial C}{\partial t} + \left(\overrightarrow{V} \cdot \overrightarrow{\nabla}\right) C = D\nabla^2 C + G. \tag{1.11}$$

1.4 Boundary Layer Flow

Prandtl showed in early 1900s that the viscous flow region could be studied by dividing the viscous flow into two parts, a region where there is flow in a thin layer near a solid wall, called the boundary layer and an outer region where friction can be neglected. They are interpreted as continuous 2D steady and incompressible continuity and momentum equation. This velocity vector will be represented as,

$$\overrightarrow{v} = u(x,y)\hat{i} + v(x,y)\hat{j}, \tag{1.12}$$

So we will have continuity equation and both components of momentum equation as,

$$u_x + v_y = 0,$$
$$uu_x + vu_y = \frac{1}{\rho}\left[-P_x + (u_{xx} + u_{yy})\,\mu\right], \tag{1.13}$$
$$uv_x + vv_y = \frac{1}{\rho}\left[-P_y + (v_{xx} + v_{yy})\,\mu\right],$$

Employing the boundary layer assumptions as,

$$u \gg v \quad , \quad \frac{\partial}{\partial y} \gg \frac{\partial}{\partial x}. \tag{1.14}$$

Eq. (1.13) implies,

$$uu_x + vu_y = \frac{1}{\rho}\left[- P_x + \mu u_{yy}\right],$$
$$P_y = 0, \tag{1.15}$$
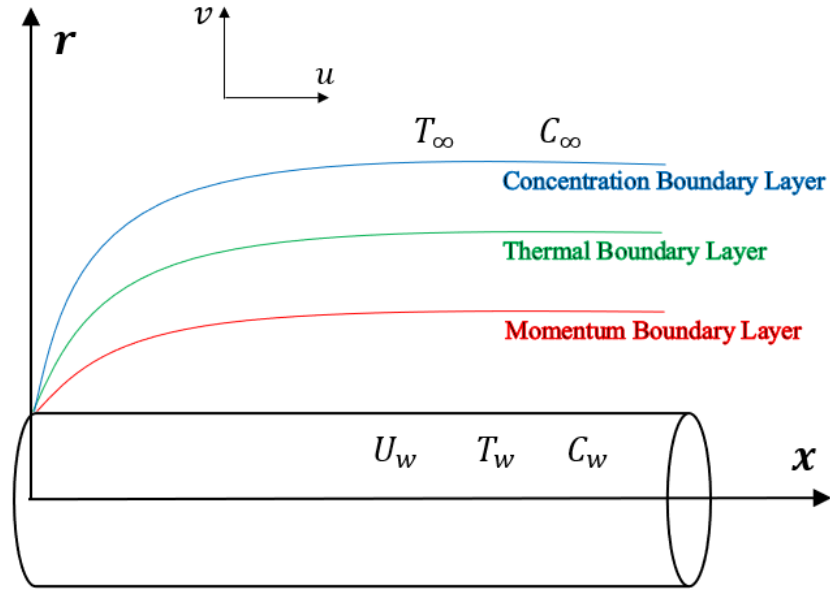
Figure 1.2: Illustration of boundary layer flow

1.4.1 Momentum Boundary Layer

In fluid dynamics, the concept of the no-slip condition is based on the assumption for viscous fluids that when they encounter a solid boundary, their velocity relative to that boundary is zero. This means that when fluid particles come into contact with a solid surface, they come to a complete halt. The absence of relative motion between the fluid and the solid surface has a cascading effect on adjacent layers of fluid particles, ultimately influencing the subsequent layers. This deceleration in velocity occurs in close proximity to the solid surface, while its impact becomes negligible as the distance from the surface increases. Within the boundary layer, the fluid velocity ranges from 0 to 0.99 times the free stream velocity, denoted as U_∞.

1.4.2 Thermal Boundary Layer

When a fluid flows over a heated surface, it creates a temperature distribution called a temperature field. This temperature field exists in a region known as the thermal boundary layer. The thickness of the thermal boundary layer is characterized by the spatial distance from the surface at which the temperature decreases to 99 % of the differential temperature between the surface and the free stream. The Prandtl number, a dimensionless parameter in fluid dynamics, plays a crucial role in determination of relative thicknesses of velocity and thermal boundary layers. Close to the heated surface, the temperature of the fluid layer is equal to the surface temperature. However, as we move away from the surface, the temperature gradually decreases until it approaches the temperature of the surrounding free stream.

1.4.3 Concentration Boundary Layer

A concentration boundary layer is a thin layer of fluid immediately adjacent to a boundary surface formed by a fluid flowing along a surface. Concentration boundary layer thickness is the distance from the surface of a solid object to the point at which the concentration of a chemical species in a fluid reaches 99% of its free-stream value. The thickness of the concentration boundary layer is affected by turbulence, usually resulting in a thicker boundary layer.

1.5 Mathematical Models

1.5.1 Buongiorno Model

In 2006, Buongiorno [23] proposed a nanofluid transport model that included four equations. The model aims to describe the behavior of nanofluids i.e fluids containing nanoparticles. Buongiorno identified seven mechanisms that could account for the relative velocity between the nanoparticles and the underlying fluid. However, he focused on two key parameters, Brownian diffusion and thermophoretic mobility as the most important factors. Based on this understanding, Buongiorno proposed a set of conservation equations incorporating these parameters to describe transport phenomena in nanofluids.

$$\vec{\nabla} \cdot \vec{V} = 0 \,,$$
$$\rho \left(\frac{\partial \vec{V}}{\partial t} + \left(\vec{V} \cdot \vec{\nabla} \right) \vec{V} \right) = -\vec{\nabla} p + \vec{\nabla} \cdot \vec{\tau} \,,$$
$$(\rho c_p) \left(\frac{\partial T}{\partial t} + \left(\vec{V} \cdot \vec{\nabla} \right) T \right) = \vec{\nabla} \cdot \vec{q} - c_p \vec{J}_p \cdot \vec{\nabla} T \,,$$
$$\left(\frac{\partial \phi}{\partial t} + \left(\vec{V} \cdot \vec{\nabla} \right) \phi \right) = -\frac{1}{\rho_p} \vec{\nabla} \cdot \vec{J}_p \,,$$

$$(1.16)$$

where heat and mass fluxes are expressed by $\boldsymbol{q}$, $\boldsymbol{J}_p$, respectively and mathemamtically defined as,

$$\vec{q} = -k_{nf}\vec{\nabla}T \, ,$$
$$\vec{J}_p = -\rho_p \left(D_B \vec{\nabla}\phi + \frac{D_T \vec{\nabla}T}{T} \right) \, , \tag{1.17}$$

among them, D_T and D_B represents the thermophoretic and Brownian diffusion coefficients, which describe the thermal motion and random diffusion motion of nanoparticles in the fluid, respectively. φ represents the concentration of nanoparticles, which indicates the number of nanoparticles per unit volume. This implies,

$$(\rho c_p) \left(\frac{\partial T}{\partial t} + \left(\vec{V} \cdot \vec{\nabla} \right) T \right) = \vec{\nabla} \cdot \left(k_{nf} \vec{\nabla}T \right) + c_p \rho_p \left(D_B \vec{\nabla}\phi + D_T \frac{\vec{\nabla}T}{T_\infty} \right) \cdot \vec{\nabla}T \, ,$$
$$\left(\frac{\partial \varphi}{\partial t} + \left(\vec{V} \cdot \vec{\nabla} \right) \varphi \right) = \vec{\nabla} \cdot \left(D_B \vec{\nabla}\varphi + D_T \frac{\vec{\nabla}T}{T_\infty} \right) \, . \tag{1.18}$$

1.5.2 Cross Fluid Model

The most common method to evaluate shear-thinning or shear-thickening fluids flow is power law model. Since the major deficiency arises due to inability of power law model to assess behaviour of fluids at very low or very high shear rates. This causes onset of class of generalized Newtonian fluids termed Cross fluids.

$$\frac{\mu - \mu_\infty}{\mu_0 - \mu_\infty} = \frac{1}{1 + (\Gamma\dot{\gamma})^n} \, , \tag{1.19}$$

where, μ_0, μ_∞, Γ, $\dot{\gamma}$, n denotes zero and infinite shear rate viscosity, relaxation time of fluid, shear rate and flow behaviour index, respectively.

1.5.3 Carreau Fluid Model

The Carreau fluid model is a mathematical model used to describe the behavior of fluids in high shear rate regions. It is named after its developer, Pierre Carreau. The model is a type of generalized Newtonian fluid model and is also considered a viscous model. It has both shear-thinning and shear-thickening properties, elastic behavior and stress growth. The Carreau fluid model can be used to simulate blood flow in narrow arteries with low shear rates. It is used for pseudoplastic and dilatant fluids and establishes a fundamental link between low shear rates (behaving like Newtonian fluids) and high shear rates (acting as power-law fluids).

$$\frac{\mu - \mu_\infty}{\mu_0 - \mu_\infty} = \left[1 + (\Gamma\dot{\gamma})^2 \right]^{\frac{n-1}{2}} \, . \tag{1.20}$$

1.6 Shear Stresses for Considered Fluid Models

1.6.1 Cross Fluid Model

For problem under consideration, shear stresses of the axisymmetric flow over the cylinder involving Cross fluid is as follows,

$$\tau_{xx} = -p + \mu_0 \frac{2\frac{\partial u}{\partial x}}{1 + \left(\Gamma\frac{\partial u}{\partial r}\right)^n} , \tag{1.21}$$

$$\tau_{rx} = \tau_{xr} = \mu_0 \frac{\frac{\partial u}{\partial r} + \frac{\partial v}{\partial x}}{1 + \left(\Gamma\frac{\partial u}{\partial r}\right)^n} , \tag{1.22}$$

$$\tau_{rr} = -p + \mu_0 \frac{2\frac{\partial v}{\partial r}}{1 + \left(\Gamma\frac{\partial u}{\partial r}\right)^n} , \tag{1.23}$$

1.6.2 Carreau Fluid Model

For problem under consideration, shear stresses of the axisymmetric flow over the cylinder involving Carreau fluid is computed.

$$\tau_{xx} = -p + \mu_0 \left(2\frac{\partial u}{\partial x}\right) \left\{ 1 + \left(\Gamma\frac{\partial u}{\partial r}\right)^2 \right\}^{\frac{n-1}{2}} , \tag{1.24}$$

$$\tau_{rx} = \tau_{xr} = \mu_0 \left(\frac{\partial u}{\partial r} + \frac{\partial v}{\partial x}\right) \left\{ 1 + \left(\Gamma\frac{\partial u}{\partial r}\right)^2 \right\}^{\frac{n-1}{2}} , \tag{1.25}$$

$$\tau_{rr} = -p + \mu_0 \left(2\frac{\partial v}{\partial r}\right) \left\{ 1 + \left(\Gamma\frac{\partial u}{\partial r}\right)^2 \right\}^{\frac{n-1}{2}} , \tag{1.26}$$

1.7 Some Non-Dimensional Parameters

1.7.1 Weissenberg Number

A dimensionless number, named after Karl Weissenberg relates elastic forces to the viscous forces. It basicly shows the relation of relaxation time with time scale of flow.

$$We = \frac{\text{elastic forces}}{\text{viscous forces}} = \frac{\lambda U}{L}. \tag{1.27}$$

where λ, U and L represents relaxation time, velocity scale and characteristic length, respectively.

1.7.2 Magnetic Parameter

The magnetic parameter is the ratio of the Lorentz force to the inertial force. The Lorentz force is the force exerted on charged particles moving at a certain speed in electric and magnetic fields. The total electromagnetic force acting on charged particles is called the Lorentz force.

$$M = \frac{\sigma B_0^2}{\rho a}.$$ (1.28)

Here, σ, B_0, a represents electrical conductivity, electric field strength and positive constant, respectively.

1.7.3 Prandtl Number

It is a dimensionless quantity that represents the ratio of kinematic viscosity and thermal diffusivity. Mathematically, it can be written as,

$$Pr = \frac{\nu}{\alpha}.$$ (1.29)

In this expression, ν signifies kinematic viscosity while, α is thermal diffusivity.

1.7.4 Schmidt Number

It is a dimensionless parameter that expresses the ratio of kinematic viscosity and the molecular diffusion coefficient. Schmidt number Sc is utilized to characterize flowing fluids where there are mass and momentum diffusion convection processes simultaneously. It is formulated as,

$$Sc = \frac{\nu}{D_B},$$ (1.30)

where, ν is kinematic viscosity and D_B is molecular diffusion coefficient.

1.7.5 Peclet Number

The Peclet number Pe is a numerical measure used to analyze the transport phenomena in a continuum. It is a dimensionless number that indicates how important advection versus diffusion is in the transport of a particular substance. A high Pe number indicates an advection-dominated flow, while a low Pe number indicates a diffusion-dominated flow. In simple terms, the Peclet number indicates the extent to which the convective motion of the substance exceeds the diffusion or vice versa.

$$Pe = \frac{\text{Transport rate of convection}}{\text{Transport rate of diffusion}} = \frac{ul}{D},$$ (1.31)

where D, l and u denotes mass diffusivity, characteristic length and flow speed, respectively.

1.8 Numerical Method

1.8.1 *bvp4c*

The MATLAB built-in package *bvp4c* is for solving boundary value problems (BVPs) of systems of ordinary differential equations. The algorithm uses an iterative structure to solve nonlinear equations and is based on the collocation method. Residuals from successive solutions are used for mesh selection and error control. Since *bvp4c* is an iterative method, the effectiveness of the algorithm will ultimately be determined by the ability to make an initial guess at the solution. The code for MATLAB is,

```
function yvector = bvpcross(t,y)     %% SystemOf1stOrderEq
    yy1 = 1/(t*(1+(1- n(j))*(we(j)*sqrt(t)*y(3))^n(j)))* ( -(2
        +(2-n(j))*(we(j)*sqrt(t)*y(3))^n(j))*0.5*y(3) - (y(1)
        *y(3) - y(2)^2 -A(j)*(y(2) + t*y(3) - Kp(j)*y(2) -M(j)
        *y(2) )*(1 + (we(j)*sqrt(t)*y(3))^n(j))^2));


    yy2 = -1/(t*(1 + epsi(j)*y(4) + 4/3*Rd(j)))*(epsi(j)*t*y
        (5)^2 + Pr(j)*(y(1)*y(5) - A(j)*t*y(5)) + Pr(j)*t*(Nb(
        j)*y(5)*y(7) + Nt(j)*y(5)^2) + Pr(j)*Q(j)*y(4) + (1+
        epsi(j)*y(4)+(4/3*Rd(j)))*y(5) );


    yy3 = -1/t*(y(7) + Sc(j)*(y(1)*y(7) - A(j)*t*y(7)) + (Nt(j
        )/Nb(j))*(t*yy2 + y(5) ) ) ;


    yvector  = [y(2); y(3); yy1; y(5); yy2; y(7); yy3];
end


hold on


function residual = bcross(y1, yinf)   %% BoundaryConditions
    residual=[y1(1);  y1(2)-1; yinf(2); y1(5) + gamma1(j)*(1 -
        y1(4))/(1+epsi(j)*y1(4) + (4/3)*Rd(j));  yinf(4);  y1
        (7)+gamma2(j)*(1 - y1(6)); yinf(6)];
end
```

```matlab
for j = 1:4
    sol1 = bvpinit(linspace(1,5,200),[0 0 0 0 0 0 0]);
    sol = bvp4c(@bvpcross, @bcross, sol1);
    eta = sol.x;
    y = sol.y;

    figure(1)
    plot(eta(1,:), y(2, :), c{j},'linewidth', 1.0)

    hold on

    ax = gca;
    ax.FontSize = 12;
    xlabel('\eta', 'fontweight', 'bold', 'fontsize', 17)
    ylabel('f^\prime(\eta)', 'fontweight', 'bold', 'fontsize', 17)

    lgd = legend({'A = -1','A = -1.2','A = -1.4','A = -1.6'},'fontsize',11,'textcolor','black')
end
```

1.9   Research Questions

The main research questions raised and justified in Chapter 2 are,

1. How does radiative heat flux affect the temperature of fluid?

2. How does porous medium affect motion of fluid?

3. How do MHD affect momentum boundary layer and velocity profile?

4. How do local Nusselt and Sherwood numbers vary due to MHD, porous medium and radiative heat flux?

Whereas, research questions raised and justified in Chapter 3 are,

1. How does MHD and porous medium effect velocity profiles of Cross and Carreau nanofluids?

2. What will be the change found in skin friction co-efficients, local Nusselt numbers, local Sherwood numbers, density of motile micro-organisms of Carreau and Cross fluid?

Chapter 2

Cross Nanofluid Flow under MHD and Radiation Effects with Variable Thermal Conductivity

2.1 Introduction

The prime concern of this study is to extend and broaden the investigations of Azam et al. [44] by instilling magnetohydrodynamics and radiation effects over stretching cylinder submerged in porous medium. In order to transform the partial differential equations of considered problem, similarity variables are utilized. The extensive problem is solved numerically by implementing built-in solver *bvp4c* of MATLAB software. Moreover, the quantities of interest such as skin friction coefficient, local Nusselt number and local Sherwood number are analyzed under the influence of different parameters and also, displayed in tabular form. While, Velocity, temperature and concentration fields are plotted in graphs.

2.2 Problem Formulation

Considering unsteady, incompressible Cross fluid flowing over porous and stretching cylinder. The cylinder having radius $a(t) = a_0\sqrt{1 - \beta t}$ that is time dependent where a_0 denotes positive constant, β represents contraction or expansion strength constant and t is time. For $\beta > 0$, there is contracting cylinder since it's radius decreases whereas, for $\beta < 0$, cylinder is expanding since it's radius increases. Buongiorno mathematical model is used in order to discuss nanofluid with thermophoresis and Brownian effects. Physically, the geometry of model is two dimensional

axisymmetric along axial (x-direction) and radial (r-direction) directions of cylinder (Figure 2.1).
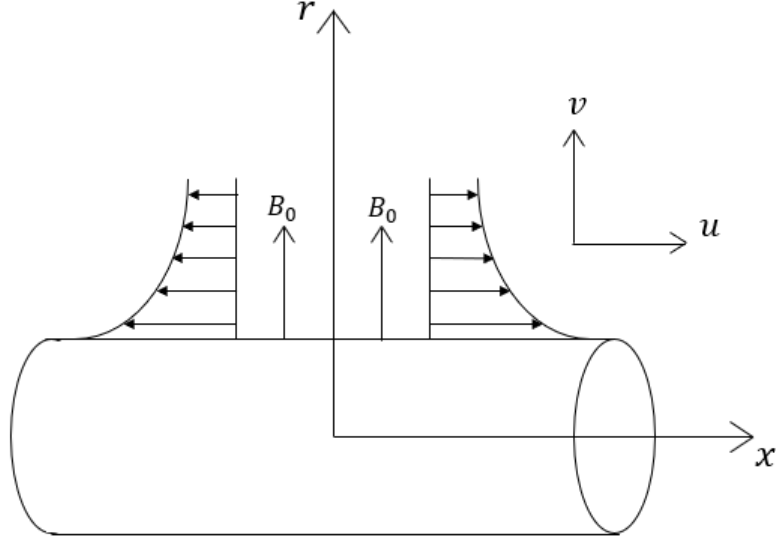
Figure 2.1: Schematic diagram of the problem.

In the current study, under variable thermal properties, temperature dependent thermal conductivity has been examined using MHD and radiation effects. The present study has been actuated in a porous medium. For variable thermal conductivity $k(T)$ [45], the mathematical relation will be,

$$k(T) = k_\infty \left[1 + \left(\frac{T - T_\infty}{\Delta T} \right) \epsilon \right], \tag{2.1}$$

where, k_∞ represents thermal conductivity distant from cylinder surface, ϵ denotes variable thermal conductivity parameter and $\Delta T = T_w - T_\infty$ is temperature gradient of fluid. Moreover, convective boundary conditions are employed in modelling the problem. For Cross fluid model [13], Cauchy stress tensor becomes,

$$\tau = -p\boldsymbol{I} + \mu \boldsymbol{A_1} \quad , \quad \mu = \frac{\mu_0}{1 + (\Gamma\dot{\gamma})^n}. \tag{2.2}$$

where, p is pressure, $\boldsymbol{I}$ identity tensor, μ apparent viscosity, $\boldsymbol{A_1}$ is first Rivilin-Ericksen tensor, μ_0 represents zero shear rate viscosity, Γ denotes time material constant and $\dot{\gamma}$ is shear rate. In order to examine the problem under consideration, $\dot{\gamma}$ in cylindrical co-ordinates will be,

$$\dot{\gamma} = \left\{ 2\left(u_x\right)^2 + 2\left(\frac{v}{r}\right)^2 + \left(u_r + v_x\right)^2 + 2\left(v_r\right)^2 \right\}^{\frac{1}{2}}. \tag{2.3}$$

The modelled equations for the considered problem are,

$$(ru)_x + (rv)_r = 0, \tag{2.4}$$

$$u_t + uu_x + vu_r = \frac{\nu}{r} u_r \left[\frac{1}{1 + (\Gamma u_r)^n} \right] + \nu \left[\frac{u_r}{1 + (\Gamma u_r)^n} \right]_r - \frac{\nu u}{k_p^*} - \frac{\sigma_1 B_0^2 u}{\rho}, \tag{2.5}$$

$$T_t + uT_x + vT_r = \frac{1}{\rho c_p} \frac{1}{r} [k(T) r T_r]_r + \tau \left[D_B C_r T_r + \frac{D_T}{T_\infty} (T_r)^2 \right] + \frac{Q_0}{\rho c_p} (T - T_\infty)$$
$$- \frac{1}{\rho c_p} \frac{1}{r} (rq_r)_r, \tag{2.6}$$

$$C_t + uC_x + vC_r = D_B \left[C_{rr} + \frac{1}{r} C_r \right] + \frac{D_T}{T_\infty} \left[T_{rr} + \frac{1}{r} T_r \right]. \tag{2.7}$$

Here, the convective boundary conditions for Eq. (2.4) - (2.7) will be,

At $r = a(t)$,

$$u = U = \frac{4\nu x}{a_0^2 (1 - \beta t)} \ , \ v = 0 \ ,$$
$$-D_m C_r = k_m (C_w - C) \ , \ -k_{eff} T_r = h_f (T_w - T) \,, \tag{2.8}$$

when $r \to \infty$, then

$$u \to 0 \ , \ T \to T_\infty \ , \ C \to C_\infty, \tag{2.9}$$

Here,

$$k_{eff} = k(T) + \frac{16\sigma^* T_\infty^3}{3k^*} \ ,$$

while, k_p^* , σ , B_0 , τ , D_B , D_T , Q_0 , D_m , h_f , k_m denotes permeability of medium, electrical conductivity of fluid, uniform magnetic field, ratio of effective heat capacity of nanoparticles and base fluids, Brownian diffusion parameter, thermophoresis diffusion parameter, heat source coefficient, molecular diffusivity, heat and mass transfer coefficient at wall, respectively. $(.)_t$, $(.)_x$ and $(.)_r$ represents derivatives with respect to t, x and r, respectively.

Moreover, radiative heat flux is expressed as q_r, which is mathematically defined as

$$q_r = -\frac{16\sigma^* T_\infty^3}{3k^*} T_r.$$

Following similarity transformations will be applied in order to get ordinary differential equations from non-linear partial differential equations (2.5) - (2.7):

$$u = \frac{4\nu x}{a_0^2 (1 - \beta t)} f'(\eta) \ , \ v = -\frac{2\nu}{a_0 \sqrt{1 - \beta t}} \frac{f(\eta)}{\sqrt{\eta}} \ , \ \eta = \left(\frac{r}{a_0} \right)^2 \frac{1}{1 - \beta t} \ ,$$

$$\theta(\eta) = (T - T_\infty)(T_w - T_\infty)^{-1} \ , \ \phi(\eta) = (C - C_\infty)(C_w - C_\infty)^{-1}. \tag{2.10}$$

Using similarity transformations defined in Eq. (2.10) , Eq. (2.5) - (2.7) becomes,

$$\{1 + (1-n)(We\sqrt{\eta}f'')^n\}\,\eta f''' + \{2 + (2-n)(We\sqrt{\eta}f'')^n\}\frac{1}{2}f'' + \{1 + (We\sqrt{\eta}f'')^n\}^2$$
$$\{f''f - A\,(f' + \eta f'') - (f')^2 - k_p f' - M f'\} = 0, \tag{2.11}$$

$$\left(1 + \epsilon\theta + \frac{4}{3}Rd\right)(\eta\theta'' + \theta') + \epsilon\eta\,(\theta')^2 + Pr\,\{Nb\phi'\theta' + Nt(\theta')^2\}\,\eta + Pr\,(f\theta' - A\eta\theta') + $$
$$PrQ\theta = 0, \tag{2.12}$$

$$(\eta\phi'' + \phi') + \frac{Nt}{Nb}\,(\theta' + \eta\theta'') + Sc\,(\phi'f - A\eta\phi') = 0. \tag{2.13}$$

The respective transformed boundary conditions will be,

$$f(1) = 0 \; , \; f'(1) = 1 \; , \; \theta'(1) = \gamma_1 \frac{(\theta(1) - 1)}{\left(1 + \epsilon\theta(1) + \frac{4}{3}Rd\right)} \; , \; \phi'(1) = \gamma_2(\phi(1) - 1), \tag{2.14}$$

$$f'(\eta) \to 0 \; , \; \theta(\eta) \to 0 \; , \; \phi(\eta) \to 0 \quad as \quad \eta \to \infty, \tag{2.15}$$

where, the dimensionless variables are We Weissenberg number, A unsteadiness parameter, K_p porosity parameter, M magnetic parameter, Q heat source parameter, Pr Prandtl number, Rd radiation parameter, Nt thermophoresis parameter, Nb Brownian motion parameter, γ_1 thermal Biot number, γ_2 solutal Biot number and Sc Schmidt number.

$$We = \frac{8\Gamma\nu x}{a_0^3(1 - \beta t)^{3/2}} \; , \quad A = \frac{a_0^2\beta}{4\nu} \; , \quad Q = \frac{Q_0 a_0^2(1 - \beta t)}{4\nu\rho c_p} \; , \; Pr = \frac{\nu}{\alpha} \; , \; Sc = \frac{\nu}{D_B} \; ,$$
$$Nt = \frac{\tau D_T(T_w - T_\infty)}{\nu T_\infty} \; , \quad Nb = \frac{\tau D_B(C_w - C_\infty)}{\nu} \; , \quad \gamma_1 = \frac{h_f}{2k_\infty}a(t) \; , \tag{2.16}$$
$$\gamma_2 = \frac{k_m}{2D_m}a(t) \; , \quad K_p = \frac{\nu x}{k_p^* U} \; , \quad M = \frac{\sigma B_0^2 x}{\rho U} \; , \quad Rd = \frac{4\sigma^* T_\infty^3}{k_\infty k^*}.$$

2.3 Physical Quantities

2.3.1 Skin Friction Coefficient

The skin friction coefficient is defined as the ratio of wall shear stress by the momentum of the free stream. In other words, it quantifies the drag force exerted on an object as a result of its interaction with a fluid. Mathematically, it is expressed as,

$$C_f = \frac{\tau_{rx}}{\frac{1}{2}\rho U^2} \; ,$$

Shear stress will be,

$$\tau_{rx} = \mu_0 \frac{u_r}{1 + (\Gamma u_r)^n} \bigg|_{r=a(t)},$$

that gives,

$$C_f \frac{x}{a(t)} = \frac{f''(1)}{1 + (We f''(1))^n} \, . \tag{2.17}$$

2.3.2 Local Nusselt Number

A dimensionless number that describes the ratio of convective to conductive heat transfer across a boundary.

$$Nu = \frac{a(t) q_w}{2k(T)(T_w - T_\infty)},$$

where, heat flux at wall is defined as

$$q_w = \left(-k(T) \left(T_r \right) + q_r \right) \bigg|_{r=a(t)},$$

this implies,

$$Nu = -\left(1 + \frac{4}{3} \frac{Rd}{(1 + \epsilon\theta(1))} \right) \theta'(1) \, . \tag{2.18}$$

2.3.3 Local Sherwood Number

A non-dimensional number that describes the ratio of convective mass transfer to the mass diffusion rate.

$$Sh = \frac{a(t) q_m}{2 D_B (C_w - C_\infty)},$$

where, mass flux at wall is illustrated as

$$q_m = -D_B \left(C_r \right) \bigg|_{r=a(t)},$$

this implies,

$$Sh = -\phi'(1) \, . \tag{2.19}$$

2.4 Numerical Methodology

Intending to handle system of non-linear ordinary differential equations, Eq. (2.11) - (2.13) will be transformed into first order ODEs. This system of differential equations will be solved numerically via MATLAB inbuilt package *bvp4c* [41]. For this purpose, derivatives will be

assumed as,

$$f = z_1 \ , \ f' = z_2 \ , \ f'' = z_3 \ , \ \theta = z_4 \ , \ \theta' = z_5 \ , \ \phi = z_6 \ , \ \phi' = z_7.$$

Consequently, seven first order differential equations will be,

$$z_1' = z_2,$$

$$z_2' = z_3,$$

$$z_3' = -\frac{\left\{(2 + (2-n))(We\sqrt{\eta}z_3)^n\right\}\frac{1}{2}z_3 + \left\{z_1 z_3 - (z_2)^2 - A(z_2 + \eta z_3) - K_p z_2 - M z_2\right\}\left\{1 + (We\sqrt{\eta}z_3)^n\right\}^2}{\left\{(1 + (1-n))(We\sqrt{\eta}z_3)^n\right\}\eta},$$

$$z_4' = z_5,$$

$$z_5' = -\frac{\epsilon\eta(z_5)^2 + Pr\eta\left\{Nbz_5 z_7 + Nt(z_5)^2\right\} + Pr\left\{z_1 z_5 - A\eta z_5\right\} + PrQz_4 + \left\{1 + \epsilon z_4 + \frac{4}{3}R_d\right\}}{\left\{1 + \epsilon z_4 + \frac{4}{3}R_d\right\}\eta},$$

$$z_6' = z_7,$$

$$z_7' = -\frac{z_7 + Sc\left\{z_1 z_7 - A\eta z_7\right\} + \frac{Nt}{Nb}\left\{z_5 + \eta z_5'\right\}}{\eta},$$

with boundary conditions,

$$z_1(1) = 0 \ , \ z_2(1) = 1 \ , \ z_5(1) = \frac{\gamma_1\left(z_4(1) - 1\right)}{1 + \epsilon z_4(1) + \frac{4}{3}Rd} \ , \ z_7(1) = \gamma_2(z_6(1) - 1),$$

$$z_2(\eta) \to 0 \ , \ z_4(\eta) \to 0 \ , \ z_6(\eta) \to 0 \qquad \text{when} \qquad \eta \to \infty.$$

2.5 Comparison and Discussion

Table 2.1: Comparing numerical results for skin friction coefficient for $n = 1$, $We = 0$

A	Fang et al.[42]	Khan et al. [43]	Azam et al. [44]	Current study
0	-1.17775	-1.17884	-1.178844	-1.178847

Table 2.2: Numerical computations for local Nusselt number when $n = 3$

A	We	Pr	Sc	ϵ	Q	γ_1	γ_2	Nt	Nb	Rd	K_p	M	Nusselt number
-1.2	0.5	6.9	2	5	0.15	0.3	0.4	0.3	0.4	0.8	0.5	0.1	0.254144
-1.4													0.258831
-1.6													0.262663
-1	0.4	6.9	2	5	0.15	0.3	0.4	0.3	0.4	0.8	0.5	0.1	0.248207
	0.6												0.248359
	0.8												0.248496
-1	0.5	7.9	2	5	0.15	0.3	0.4	0.3	0.4	0.8	0.5	0.1	0.25252
		8.9											0.256091
		10											0.259408
-1	0.5	6.9	3	5	0.15	0.3	0.4	0.3	0.4	0.8	0.5	0.1	0.248545
			4										0.248791
			5										0.248997
-1	0.5	6.9	2	0	0.15	0.3	0.4	0.3	0.4	0.8	0.5	0.1	0.289815
				10									0.217781
				20									0.175871
-1	0.5	6.9	2	5	0.45	0.3	0.4	0.3	0.4	0.8	0.5	0.1	0.246197
					0.75								0.243757
					1.15								0.239736
-1	0.5	6.9	2	5	0.15	0.4	0.4	0.3	0.4	0.8	0.5	0.1	0.312882
						0.5							0.370688
						0.6							0.422699
-1	0.5	6.9	2	5	0.15	0.3	0.5	0.3	0.4	0.8	0.5	0.1	0.247719
							0.6						0.247178
							0.7						0.24666
-1	0.5	6.9	2	5	0.15	0.3	0.4	0.4	0.4	0.8	0.5	0.1	0.247993
								0.5					0.247698
								0.6					0.247400
-1	0.5	6.9	2	5	0.15	0.3	0.4	0.3	0.4	0.8	0.5	0.1	0.248286
									0.7				0.246234
									0.9				0.244814
-1	0.5	6.9	2	5	0.15	0.3	0.4	0.3	0.4	0.2	0.5	0.1	0.243345
										0.4			0.245247
										0.6			0.246868
-1	0.5	6.9	2	5	0.15	0.3	0.4	0.3	0.4	0.8	1	0.1	0.248235
											1.5		0.248194
											2.5		0.24813
-1	0.5	6.9	2	5	0.15	0.3	0.4	0.3	0.4	0.8	0.5	0.2	0.248275
												0.6	0.248235
												1	0.248201

2.5.1 Analysis of Results

The results found in response to the research questions mentioned initially are represented via graphs and tables. While responding to the research questions, Figure 2.2 is resolving question 1, Figure 2.3 is drawn to answer question 2, whereas Figure 2.4 is responding to question 3. In

order to minimize research question 4, Table 2.2 - 2.3 is presented.

Table 2.3: Numerical computations for local Sherwood number when $n = 3$

A	We	Pr	Sc	ϵ	Q	γ_1	γ_2	Nt	Nb	Rd	K_p	M	Sherwood number
-1.2	0.5	6.9	2	5	0.15	0.3	0.4	0.3	0.4	0.8	0.5	0.1	0.350566
-1.4													0.354888
-1.6													0.358521
-1	0.4	6.9	2	5	0.15	0.3	0.4	0.3	0.4	0.8	0.5	0.1	0.345223
	0.6												0.345450
	0.8												0.345670
-1	0.5	7.9	2	5	0.15	0.3	0.4	0.3	0.4	0.8	0.5	0.1	0.345169
		8.9											0.344911
		10											0.344674
-1	0.5	6.9	3	5	0.15	0.3	0.4	0.3	0.4	0.8	0.5	0.1	0.358814
			4										0.366762
			5										0.372050
-1	0.5	6.9	2	0	0.15	0.3	0.4	0.3	0.4	0.8	0.5	0.1	0.344481
				10									0.346050
				20									0.347183
-1	0.5	6.9	2	5	0.45	0.3	0.4	0.3	0.4	0.8	0.5	0.1	0.345484
					0.75								0.345660
					1.15								0.345952
-1	0.5	6.9	2	5	0.15	0.4	0.4	0.3	0.4	0.8	0.5	0.1	0.342885
						0.5							0.340629
						0.6							0.338550
-1	0.5	6.9	2	5	0.15	0.3	0.5	0.3	0.4	0.8	0.5	0.1	0.419685
							0.6						0.490020
							0.7						0.556657
-1	0.5	6.9	2	5	0.15	0.3	0.4	0.4	0.4	0.8	0.5	0.1	0.342438
								0.5					0.339553
								0.6					0.336682
-1	0.5	6.9	2	5	0.15	0.3	0.4	0.3	0.4	0.8	0.5	0.1	0.345338
									0.7				0.349189
									0.9				0.350331
-1	0.5	6.9	2	5	0.15	0.3	0.4	0.3	0.4	0.2	0.5	0.1	0.339851
										0.4			0.342242
										0.6			0.343996
-1	0.5	6.9	2	5	0.15	0.3	0.4	0.3	0.4	0.8	1	0.1	0.345250
											1.5		0.345178
											2.5		0.345067
-1	0.5	6.9	2	5	0.15	0.3	0.4	0.3	0.4	0.8	0.5	0.2	0.345319
												0.6	0.345250
												1	0.345191

2.5.2 Discussion of Results

The findings derived in response to the posed research queries are subjected to an analysis and deliberation in this section. Figure 2.2 elucidates variation in radiation parameter on concentration field. Increase in Rd causes rise in $\theta(\eta)$ and their boundary layer thickness. Figure 2.3 represents the variation in velocity profile due to porosity parameter K_p. When K_p rises, $f'(\eta)$ reduces. Physically, porous medium implements higher restriction on fluid flow causing it to move slowly. The behavior of magnetic parameter M on $f'(\eta)$ is depicted in Figure 2.4. The magnetic field parameter generates drag force that dampens the fluid velocity. In Table 2.2 and 2.3, it is noticed that local Nusselt and Sherwood number is rising function of Rd. Heat and mass transfer rate diminishes little bit when K_p and M uplifted.
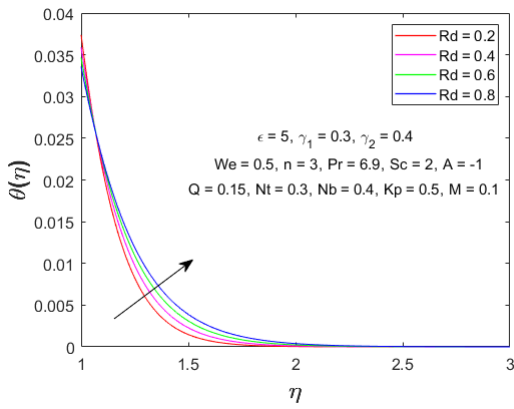

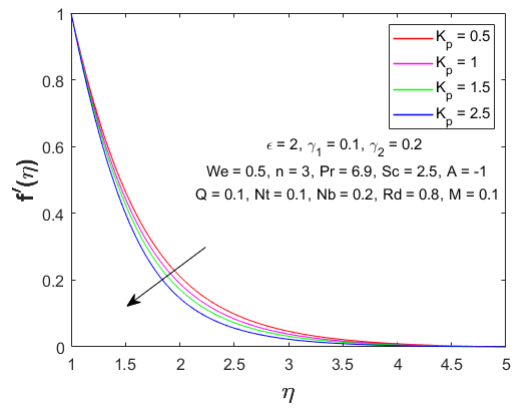Figure 2.2: Effect of radiation parameter on temperature curve.

Figure 2.3: Impact on velocity curve due to porosity parameter.

2.5.3 Investigation of various other parameters

The computations found as result of numerical procedure are featured in Table 2.1 that depicts comparison of present numerical study with previous literature in order to validate the numerical simulations.

Table 2.2 - 2.3 highlights the numeric outcomes for heat and mass transfer rate by varying the dimensionless parameters such as unsteadiness parameter A, Weissenberg number We, Prandtl number Pr, Schmidt number Sc, thermal conductivity parameter ϵ, thermal Biot number γ_1, solutal Biot number γ_2, heat source parameter Q, thermophoresis parameter Nt, Brownian parameter Nb with magnetic parameter M, radiation parameter Rd and porosity parameter K_p. It is found in Table 2.2 and 2.3 that local Nusselt number enhancing function of γ_1 and local Sherwood number is rising function of A, ϵ, Q, γ_2 and Nb. Heat transfer rate diminishes when ϵ, Q, γ_2, Nt and Nb increases, whereas rate of mass transfer reduces when γ_1 and Nt uplifted.
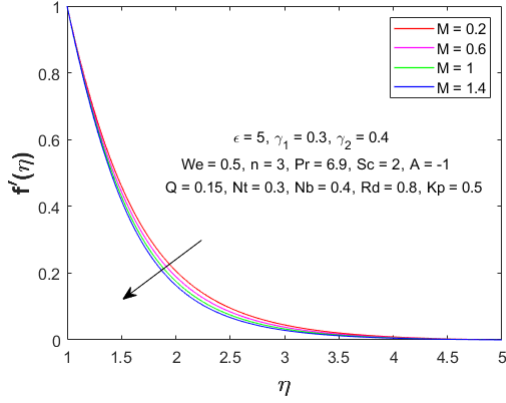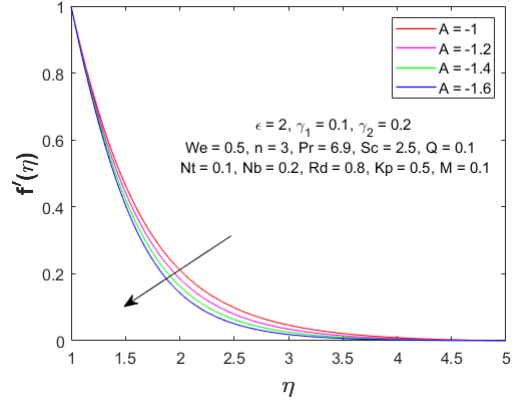
23

Figure 2.4: Impact of M on $f'(\eta)$.

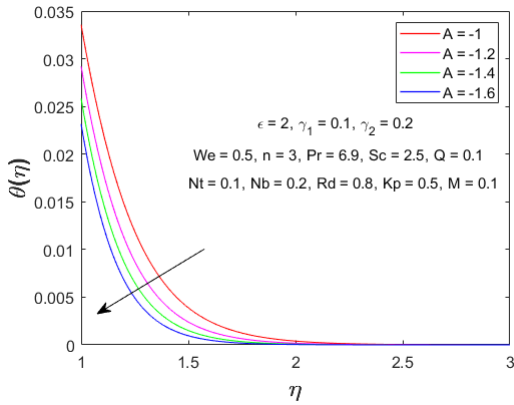Figure 2.5: Velocity curves for different A.

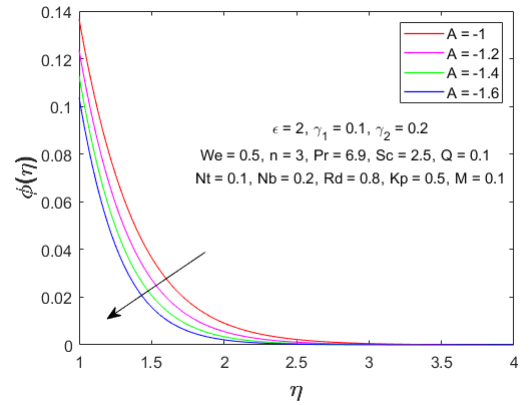Figure 2.6: Temperature curves for varying unsteadiness parameter.

Figure 2.7: Concentration curves for varying unsteadiness parameter.

The influence of the remaining parameters are presented and discussed here.

Figure 2.5 illustrates the effect of unsteadiness parameter A on velocity whereas, temperature and concentration fields are depicted by Figure 2.6 and 2.7, respectively. It indicates that with the decrease in value of A, velocity, temperature, concentration profiles and their respective boundary layer thickness diminishes. In fact, unsteadiness increases when β is becoming far smaller than 0 causing lower flow strength, $\theta(\eta)$ and $\phi(\eta)$.

The variation in Prandtl number Pr on $\theta(\eta)$ has been depicted through Figure 2.8. Physically, when Prandtl number enhances, there is an improvement in momentum diffusivity relative to thermal diffusivity, that diminishes $\theta(\eta)$.

The influence of Schmidt number Sc on nanoparticle concentration is illustrated through Figure 2.9. Since, increase in Schmidt number lowers the concentration field and respective boundary layer. Physically, higher Sc implies enhanced momentum diffusivity relative to mass diffusivity that returns depressed $\phi(\eta)$.
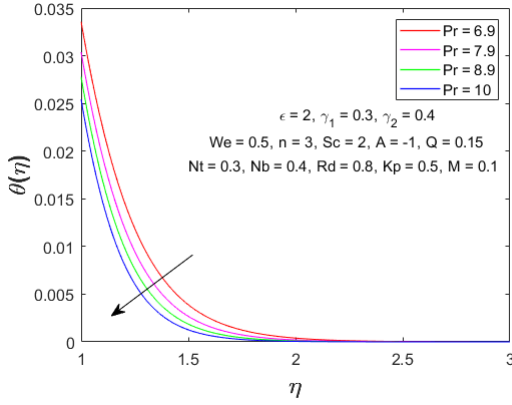
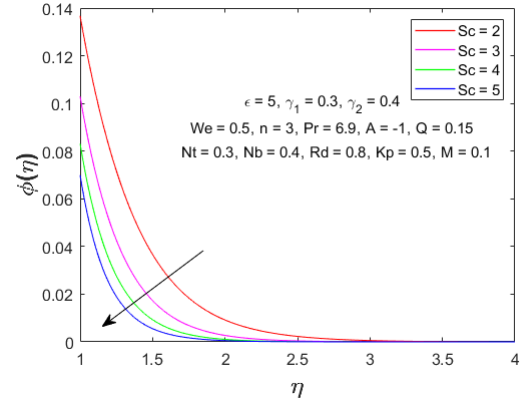Figure 2.8: Modulation of temperature profile by the Prandtl number.

Figure 2.9: Modulation of concentration profile by Schmidt number.
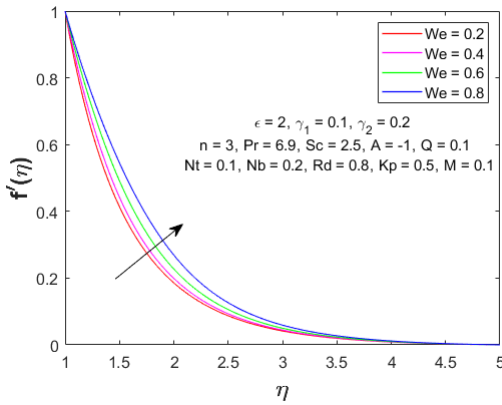

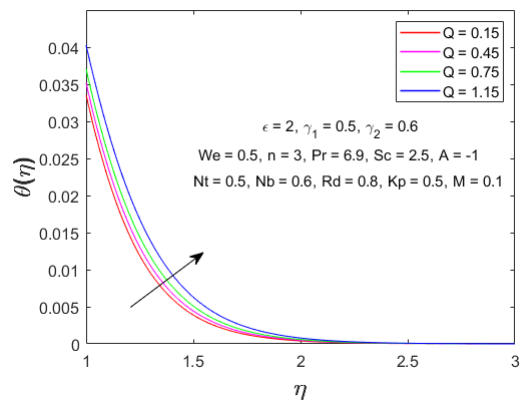Figure 2.10: Velocity curves for different Weissenberg number.

Figure 2.11: Effect of heat source parameter on $\theta(\eta)$.

Figure 2.10 indicates behavior of Weissenberg number on velocity profile. Smaller We implies viscous forces of the flow dominates. So, when Weissenberg number increases from 0.2 till 0.8, the dominating viscous forces of flow are becoming weaker that causes enhanced flow velocity.

The variation of temperature curve due to change in heat source parameter is demonstrated in Figure 2.11. With any increase in Q, heat will be produced causing enhanced temperature profile.

The impact of thermal conductivity parameter ϵ on temperature and concentration profiles is depicted through Figure 2.12 and 2.13, respectively. It is observed that, at constant thermal conductivity parameter $\epsilon = 0$ temperature and nanoparticle concentration is larger when comparing to varying thermal conductivity. The temperature diminishes closer to the surface of cylinder due to increase in ϵ. While, the temperature curve far away from cylinder shows opposite trend, enhancing values of thermal conductivity parameter leads to higher temperature field. Whereas,

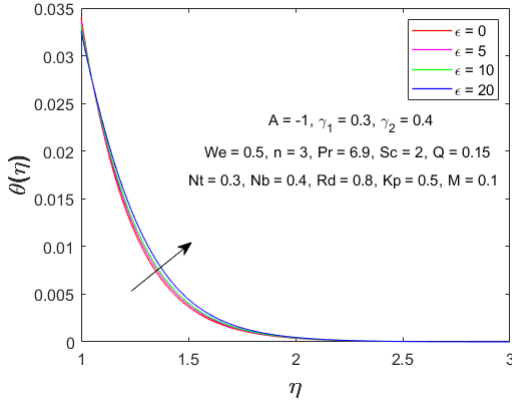decline in concentration profile is observed.

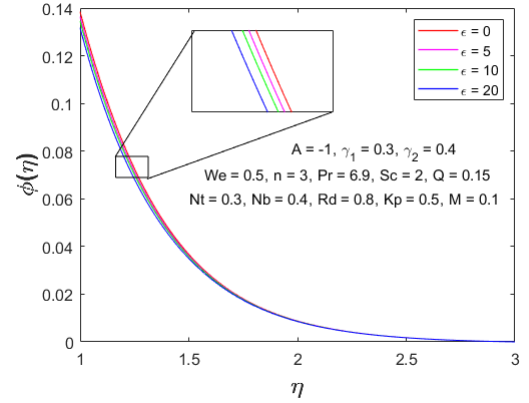Figure 2.12: Influence of thermal conductivity parameter on $\theta(\eta)$.

Figure 2.13: Influence of thermal conductivity parameter on $\phi(\eta)$.
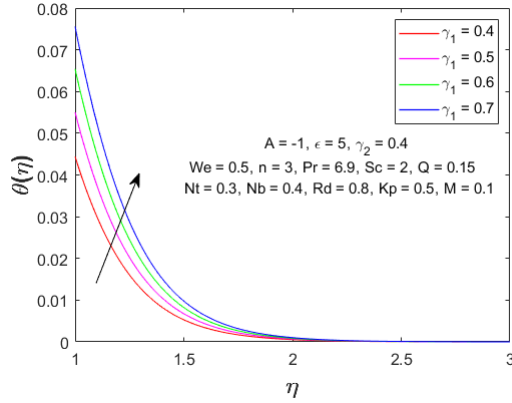
Figure 2.14: Change in $\theta(\eta)$ due to γ_1.
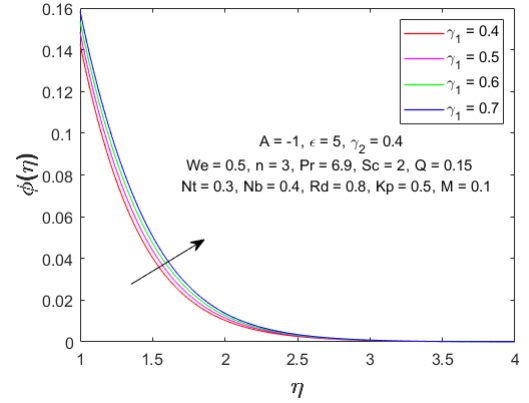
Figure 2.15: Change in $\phi(\eta)$ due to γ_1.

The influence of thermal Biot number γ_1 on temperature and nanoparticle concentration profiles is depicted in Figure 2.14 and 2.15, respectively. With the increase in γ_1, temperature and concentration fields increases. When $\gamma_1 = 0$, the surface of cylinder will be completely isolated and then, thermal resistance inside cylinder is infinitely large relative to its thermal layer thickness. So, convective heat transfer discontinues.

Figure 2.16 indicates the impact of γ_2 on concentration curve. Whenever, solutal Biot number rises, it enhances molecular diffusivity of the flow then, concentration profile increases.

Figure 2.17 and 2.18 illustrates influence of Brownian parameter whereas, the behavior of thermophoresis is shown in Figure 2.19, respectively. The higher flow strength is generated away from the stretching surface due to temperature gradient in affect of thermophoretic force. The accelerated fluid flowing from the stretching surface with thermophoretic force results in the increase of temperature in boundary layer leading to the higher boundary layer thickness of $\phi(\eta)$.

Greater thermophoresis parameter means the temperature gradient between surface and ambient rises, which gives enriched fluid concentration. On the other hand, when Nb uplifts, it causes considerable rise in $\theta(\eta)$ and fall in $\phi(\eta)$. It happens since increase in Brownian parameter results higher random motion of nanoparticles implying diminished concentration of nanoparticles.
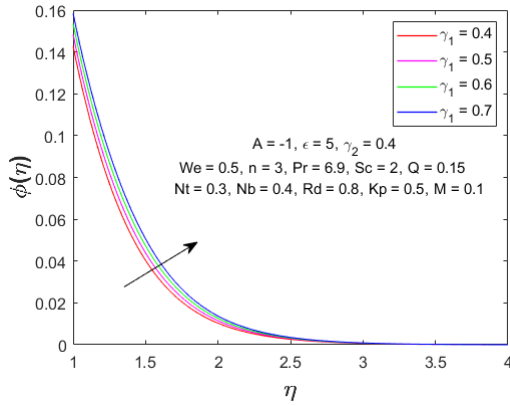

Figure 2.16: Change in $\phi(\eta)$ due to solutal Biot number.
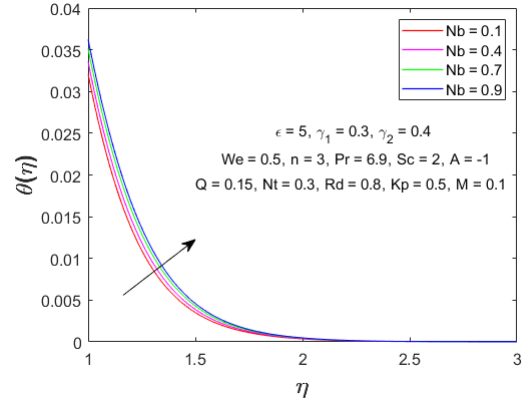
Figure 2.17: Variation of $\theta(\eta)$ due to Brownian parameter.
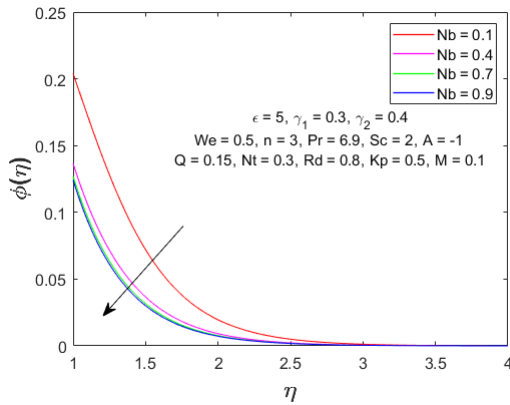
Figure 2.18: Variation of $\phi(\eta)$ due to Brownian parameter.
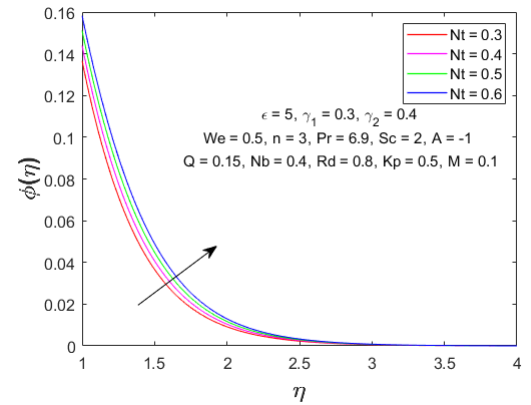
Figure 2.19: Variation of $\phi(\eta)$ due to thermophoresis parameter.

Chapter 3

Comparative Analysis of Cross and Carreau Nanofluid Flow Containing Motile Microorganisms

3.1 Introduction

This chapter covers the comparative analysis of two generalized non-Newtonian fluid models under the effects of thermal radiation, magnetohydrodynamics and Arrhenius activation energy. The flow model involves complex and highly nonlinear ordinary differential equations that have been solved using the MATLAB built-in package *bvp4c*. The study evaluated the enhancement of heat and mass transport by considering the effects of Brownian motion and thermophoresis. It presents and explains graphical profiles of the velocity, temperature, concentration and density of microorganisms based on appropriate parameters. Finally, skin friction coefficient, the rates of heat transfer, mass transfer and motile density are analyzed and discussed using the graphs and tables.

3.2 Problem Formulation

Assuming an incompressible, steady laminar flow of 2D bionanofluid via stretching cylindrical geometry in axial direction. The cylinder immersed in porous medium is subjected to MHD, thermal radiation, heat source or sink along with the presence of Arrhenius activation energy.

The geometry of the problem is kept at constant temperature, denoted as T_w and fixed concentration of nanoparticles, represented as C_w while, surrounding environmental conditions are characterized by ambient temperature and concentration, symbolized as T_∞ and C_∞, respectively (Figure 3.1). Here, $a(t) = a_0\sqrt{1 - \beta t}$ is the radius of cylinder with β representing strength of stretching constant.
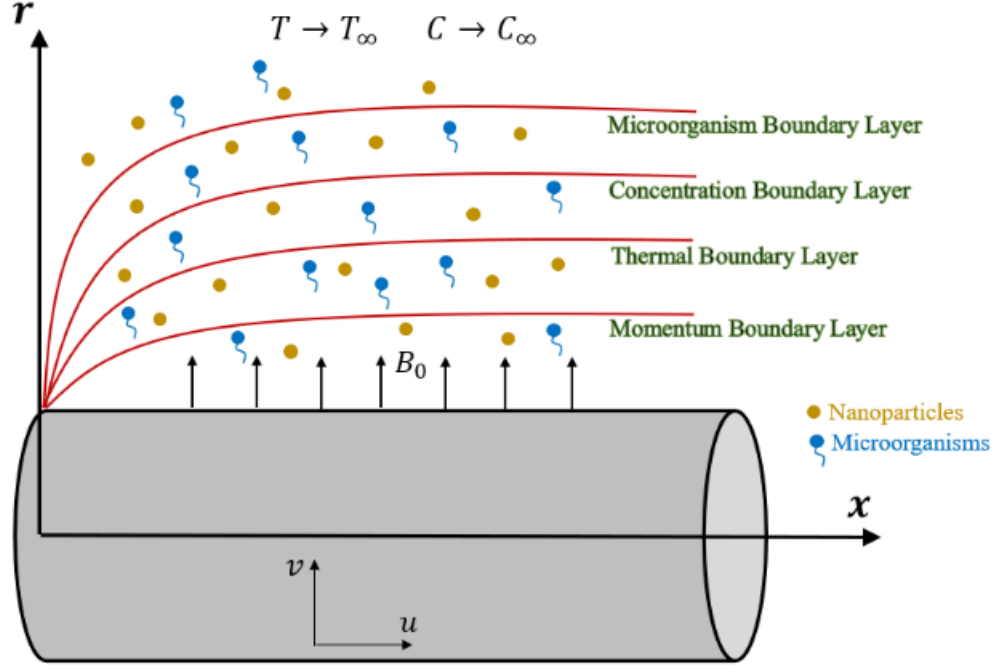
Figure 3.1: Illustrative configuration of the problem.

The flow equations for the current problem will be as follows,

$$\frac{\partial}{\partial x}(ru) + \frac{\partial}{\partial r}(rv) = 0, \tag{3.1}$$

For Carreau nanofluid, momentum equation is

$$\frac{\partial u}{\partial t} + u\frac{\partial u}{\partial x} + v\frac{\partial u}{\partial r} = \nu\left[\frac{1}{r}\frac{\partial u}{\partial r} + \frac{\partial^2 u}{\partial r^2} + \left(\frac{n-1}{2r}\right)\Gamma^2\left(\frac{\partial u}{\partial r}\right)^3 + 3\left(\frac{n-1}{2}\right)\Gamma^2\left(\frac{\partial u}{\partial r}\right)^2\frac{\partial^2 u}{\partial r^2}\right]$$
$$-\frac{\sigma_1 B_0^2 u}{\rho} - \frac{\nu u}{K_p^*} + \frac{1}{\rho}\wp B_T(T - T_\infty) + \frac{1}{\rho}\wp B_C(C - C_\infty), \tag{3.2}$$

29

For Cross nanofluid, momentum equation will be,

$$\frac{\partial u}{\partial t} + u\frac{\partial u}{\partial x} + v\frac{\partial u}{\partial r} = \frac{\nu}{r}\frac{\partial u}{\partial r}\left[\frac{1}{1+\left(\Gamma\frac{\partial u}{\partial r}\right)^n}\right] + \nu\frac{\partial}{\partial r}\left[\frac{\frac{\partial u}{\partial r}}{1+\left(\Gamma\frac{\partial u}{\partial r}\right)^n}\right] \tag{3.3}$$
$$+\frac{1}{\rho}\wp B_T(T-T_\infty) + \frac{1}{\rho}\wp B_C(C-C_\infty) - \frac{\sigma_1 B_0^2 u}{\rho} - \frac{\nu u}{K_p^*},$$

$$\frac{\partial T}{\partial t} + u\frac{\partial T}{\partial x} + v\frac{\partial T}{\partial r} = \alpha\left(\frac{\partial^2 T}{\partial r^2} + \frac{1}{r}\frac{\partial T}{\partial r}\right) + \tau\left(D_B\frac{\partial C}{\partial r}\frac{\partial T}{\partial r} + \frac{D_T}{T_\infty}\left(\frac{\partial T}{\partial r}\right)^2\right) \tag{3.4}$$
$$+\frac{Q_0}{\rho c_p}(T-T_\infty) - \frac{1}{\rho c_p}\frac{1}{r}\frac{\partial}{\partial r}(rq_r),$$

$$\frac{\partial C}{\partial t} + u\frac{\partial C}{\partial x} + v\frac{\partial C}{\partial r} = D_B\left(\frac{\partial^2 C}{\partial r^2} + \frac{1}{r}\frac{\partial C}{\partial r}\right) + \frac{D_T}{T_\infty}\left(\frac{\partial^2 T}{\partial r^2} + \frac{1}{r}\frac{\partial T}{\partial r}\right) \tag{3.5}$$
$$-k_r(C-C_\infty)\left(\frac{T}{T_\infty}\right)^m \exp\left(\frac{-Ea}{K_B T}\right),$$

$$\frac{\partial N}{\partial t} + u\frac{\partial N}{\partial x} + v\frac{\partial N}{\partial r} + \frac{bw_c}{(C_w-C_\infty)}\frac{1}{r}\frac{\partial}{\partial r}\left(N\left(r\frac{\partial C}{\partial r}\right)\right) = \frac{D_n}{r}\frac{\partial}{\partial r}\left(r\frac{\partial N}{\partial r}\right), \tag{3.6}$$

with appropriate boundary conditions as,

At $r = a(t)$,

$$u = U = \frac{4\nu x}{a_0^2(1-\beta t)} , \quad v = 0 , \quad N = N_w ,$$
$$-D_m\frac{\partial C}{\partial r} = m_t(C_w - C) , \quad -k_{eff}\frac{\partial T}{\partial r} = h_t(T_w - T) , \tag{3.7}$$

when $r \to \infty$, then

$$u \to 0 , \ T \to T_\infty , \ C \to C_\infty , \ N \to N_\infty, \tag{3.8}$$

Here,

$$k_{eff} = k + \frac{16\sigma^* T_\infty^3}{3k^*} ,$$

while σ_1, $\wp$, B_T, B_C, B_0, K_p^*, α, τ, q_r, k_r, m, Ea, K_B, N, b, w_c, D_n, D_m, m_t, h_t and k shows electrical conductivity of fluid, gravitational acceleration, volumetric thermal expansion coefficient, volumetric solutal expansion coefficient, uniform magnetic field, permability of porous medium, thermal diffusivity, ratio of effective heat capacity of nanoparticles and base fluids, radiative heat flux, chemical reaction rate, fitted rate constant, Arrhenius activation energy, Boltzmann constant, concentration of micro-organisms, chemotaxis constant, maximum cell swimming speed, diffusivity of micro-organisms, molecular diffusivity, mass transfer co-efficient, heat transfer co-efficient and constant thermal conductivity, respectively.

Similarity transformations suitable for given problem are defined as,

$$u = \frac{4\nu x}{a_0^2\,(1-\beta t)}g'(\xi) \ , \ v = -\frac{2\nu}{a_0\sqrt{1-\beta t}}\frac{g(\xi)}{\sqrt{\xi}} \ , \ \xi = \left(\frac{r}{a_0}\right)^2\frac{1}{1-\beta t} \ ,$$

$$\vartheta(\xi) = (T-T_\infty)(T_w-T_\infty)^{-1} \ , \ \varphi(\xi) = (C-C_\infty)(C_w-C_\infty)^{-1} \ ,$$

$$\chi(\xi) = (N-N_\infty)(N_w-N_\infty)^{-1}. \tag{3.9}$$

With the intention of transforming partial differential equations written in Eq. (3.2) - (3.6) into ordinary differential equations, we will utilize Eq. (3.9) and get,

$$\xi g''' \left\{1 + 3\left(\frac{n-1}{2}\right)(Weg'')^2\,\xi\right\} + g''\left\{1 + (n-1)(Weg'')^2\,\xi\right\} - A\,(g' + \xi g'') - (g')^2$$
$$+ g''g + G_t\vartheta + G_s\varphi - g'\,(M+K_p) = 0, \tag{3.10}$$

$$\frac{1}{2}g''\left\{2 + (2-n)\left(We\sqrt{\xi}g''\right)^n\right\} + \xi g'''\left\{1 + (1-n)\left(We\sqrt{\xi}g''\right)^n\right\} + \left\{\left(1 + \left(We\sqrt{\xi}g''\right)^n\right)^2\right\}$$
$$\left\{g''g - A\,(g' + \xi g'') - (g')^2 + G_t\vartheta + G_s\varphi - g'\,(M+K_p)\right\} = 0, \tag{3.11}$$

$$\left[1 + \frac{4}{3}Rd\right](\vartheta' + \xi\vartheta'') + Pr\left\{\xi\left(Nb\varphi'\vartheta' + Nt\,(\vartheta')^2\right) + \vartheta'\,(g-A\xi) + Q\vartheta\right\} = 0, \tag{3.12}$$

$$(\xi\varphi'' + \varphi') + \frac{Nt}{Nb}(\vartheta' + \xi\vartheta'') - Sc\,\sigma\,\varphi\,(1+\delta\vartheta)^m\exp\left(\frac{-E}{1+\delta\vartheta}\right) + Sc\,(g-A\xi)\,\varphi' = 0, \tag{3.13}$$

$$\chi' + \xi\chi'' - Sb\,(A\xi+g)\,\chi' - Pe\left\{\chi'\varphi' + (\chi+\omega)\,(\varphi' + \xi\varphi'')\right\} = 0. \tag{3.14}$$

The boundary conditions, transformed correspondingly with Eq. (3.10) - (3.14) are delineated as follows:

$$g(1) = 0 \ , \ g'(1) = 1 \ , \ \vartheta'(1) = \frac{\gamma_1\,(\vartheta(1)-1)}{(1 + \frac{4}{3}\,Rd)} \ , \ \varphi'(1) = \gamma_2\,(\varphi(1)-1) \ , \ \chi(1) = 1,$$

$$g'(\xi) \to 0 \ , \quad \vartheta(\xi) \to 0 \ , \quad \varphi(\xi) \to 0 \ , \quad \chi(\xi) \to 0 \quad as \quad \xi \to \infty. \tag{3.15}$$

The dimensionless parameters appearing are,

$$We = \frac{8\Gamma\nu x}{a_0^3(1-\beta t)^{3/2}} \ , \quad A = \frac{a_0^2\beta}{4\nu} \ , \quad G_t = \frac{\wp B_T x}{\rho U^2}(T_w - T_\infty) \ ,$$

$$G_s = \frac{\wp B_C x}{\rho U^2}(C_w - C_\infty) \ , \quad Q = \frac{Q_0 a_0^2(1-\beta t)}{4\nu\rho c_p} \ , \quad Sc = \frac{\nu}{D_B} \ ,$$

$$Nt = \frac{\tau D_T(T_w - T_\infty)}{\nu T_\infty} \ , \quad Nb = \frac{\tau D_B(C_w - C_\infty)}{\nu} \ , \quad \gamma_1 = \frac{h_t}{2k}a(t) \ ,$$

$$\gamma_2 = \frac{m_t}{2D_m}a(t) \ , \quad M = \frac{\sigma_1 B_0^2 x}{\rho U} \ , \quad Rd = \frac{4\sigma^* T_\infty^3}{k\,k^*} \ , \quad Pr = \frac{\nu}{\alpha} \ ,$$

$$\delta = \frac{T_w - T_\infty}{T_\infty} \ , \quad K_p = \frac{\nu x}{k_p^* U} \ , \quad \sigma = \frac{k_r x}{U} \quad , \quad E = \frac{Ea}{K_B T_\infty} \ ,$$

$$Sb = \frac{\nu}{D_n} \quad , \quad Pe = \frac{bw_c}{D_n} \quad , \quad \omega = \frac{N_\infty}{N_w - N_\infty} \ .$$

(3.16)

Here, We is Weissenberg number, A denotes unsteadiness parameter, Pr shows Prandtl number, G_t represents temperature buoyancy parameter, G_s depicts concentration buoyancy parameter, Q defines heat source parameter, Sc is Schmidt number, thermophoresis parameter is depicted by Nt , Brownian parameter is illustrated by Nb, γ_1 is for thermal Biot number, γ_2 for solutal Biot number, M specifies Magnetic parameter, Rd refers to radiation parameter, δ indicates temperature difference, K_p is porosity parameter, σ shows chemical reaction parameter, activation parameter is denoted by E, Sb defines bioconvection Schmidt number, Pe is Peclet number, ω represents bioconvection parameter (motile microorganism difference parameter)

3.3   Physical Quantities

3.3.1   Skin Friction Coefficient

The quantity of interest is,

$$C_f = \frac{\tau_{rx}}{\frac{1}{2}\rho U^2} \ ,$$

where, τ_{rx} is wall shear stress

$$\text{Carreau fluid:} \qquad \tau_{rx} = \left[\mu_0\left(\frac{\partial u}{\partial r}\right)\left(1 + \left(\Gamma\frac{\partial u}{\partial r}\right)^2\right)^{\frac{n-1}{2}}\right]_{r=a(t)} \ ,$$

$$\text{Cross fluid:} \qquad \tau_{rx} = \mu_0\frac{\dfrac{\partial u}{\partial r}}{1 + \left(\Gamma\dfrac{\partial u}{\partial r}\right)^n}\bigg|_{r=a(t)} \ ,$$

The dimensionless coefficient of skin friction for both fluids is expressed as,

$$\text{Carreau fluid:} \qquad C_f \frac{x}{a(t)} = g''(1)\left(1 + (Weg''(1))^2\right)^{\frac{n-1}{2}}, \qquad (3.17)$$

$$\text{Cross fluid:} \qquad C_f \frac{x}{a(t)} = \frac{g''(1)}{1 + (Weg''(1))^n} . \qquad (3.18)$$

3.3.2 Local Nusselt Number

To calculate the local Nusselt number, we have formula

$$Nu = \frac{a(t)q_w}{2k(T_w - T_\infty)},$$

where, q_w is heat flux at wall which is defined by Fourier's law of heat conduction as,

$$q_w = -\left(k + \frac{16\sigma^* T_\infty^3}{3k^*}\right)\left(\frac{\partial T}{\partial r}\right)\bigg|_{r=a(t)},$$

Thus, rate of heat transfer Nu equation becomes,

$$Nu = -\left(1 + \frac{4}{3}Rd\right)\vartheta'(1) . \qquad (3.19)$$

3.3.3 Local Sherwood Number

To compute local Sherwood number, we have

$$Sh = \frac{a(t)q_m}{2D_B(C_w - C_\infty)},$$

where, q_m shows mass flux of nanoparticles at surface which is determined using Fick's law of diffusion as,

$$q_m = -D_B\left(\frac{\partial C}{\partial r}\right)\bigg|_{r=a(t)},$$

This implies non-dimensional mass transfer rate Sh equation as follows,

$$Sh = -\varphi'(1) . \qquad (3.20)$$

3.3.4 Local Density of Motile Micro-organisms

In order to demonstrate the local density of micro-organisms, we measure Nn as

$$Nn = \frac{xj_w}{D_n(N_w - N_\infty)},$$

where, j_w depicts mass flux of motile microorganisms at wall.

$$j_w = -D_n \left(\frac{\partial N}{\partial r} \right) \bigg|_{r=a(t)} ,$$

Therefore, dimensionless Nn will be written as,

$$Nn = -\chi'(1) . \tag{3.21}$$

3.4 Numerical Methodology

When the boundary value problem needs to solve numerically, it is necessary to convert higher order differential equations into system of first order ordinary differential equations. For this purpose, Eq. (3.10) - (3.14) are first transformed into system of first order ODEs so that, it will then be solved numerically by utilizing MATLAB solver *bvp4c* [41]. Here, we are assuming derivatives as,

$$g = z_1 , \quad g' = z_2 , \quad g'' = z_3 , \quad \vartheta = z_4 , \quad \vartheta' = z_5 ,$$
$$\varphi = z_6 , \quad \varphi' = z_7 , \quad \chi = z_8 , \quad \chi' = z_9.$$

Subsequently, nine first order differential equations for each Carreau and Cross fluid are,

$$z_1' = z_2,$$

$$z_2' = z_3,$$

$$z_3' = \begin{bmatrix} \begin{bmatrix} -z_3 \left(1 + (n-1)\xi (Wez_3)^2\right) + A(z_2 + \xi z_3) + (z_2)^2 - z_3 z_1 + z_2 (M + K_p) \\ -G_t z_4 - G_s z_6 \end{bmatrix} \begin{bmatrix} \xi \left(1 + 3\left(\frac{n-1}{2}\right)\xi (Wez_3)^2\right) \end{bmatrix}^{-1} \\ \text{(Carreau fluid)} \\ \\ \begin{bmatrix} -\frac{z_3}{2}\left(2 + (2-n)\left(We\sqrt{\xi}z_3\right)^n\right) + \begin{bmatrix} A(z_2 + \xi z_3) - z_3 z_1 + (z_2)^2 + z_2 (M + K_p) \\ -Gtz_4 - Gsz_6 \end{bmatrix} \left(1 + (We\sqrt{\xi}z_3)^n\right)^2 \end{bmatrix} \begin{bmatrix} \xi \left(1 + (1-n)\left(We\sqrt{\xi}z_3\right)^n\right) \end{bmatrix}^{-1} \\ \text{(Cross fluid)} \end{bmatrix},$$

$$z_4' = z_5,$$

$$z_5' = \left[\xi\left(1 + \frac{4}{3}Rd\right)\right]^{-1}\left[-Pr\left\{\xi\left(Nbz_5 z_7 - Nt(z_5)^2\right) + z_5(z_1 - A\xi) + Qz_4\right\} + \left(1 + \frac{4}{3}Rd\right)z_5\right],$$

$$z_6' = z_7,$$

$$z_7' = \frac{1}{\xi}\left[-\frac{Nt}{Nb}\left(z_5 + \xi z_5'\right) + \sigma Sc\left(1 + \delta z_4\right)^m z_6 \exp\left(\frac{-E}{1 + \delta z_4}\right) - Sc\left(z_1 - A\xi\right)z_7 - z_7\right],$$

$$z_8' = z_9,$$

$$z_9' = \frac{1}{\xi}\left[-z_9 + Sb\left(A\xi + z_1\right)z_9 + Pe\left\{z_9 z_7 + \left(z_8 + \omega\right)\left(z_7 + \xi z_7'\right)\right\}\right],$$

with boundary conditions,

$$z_1(1) = 0 \; , \; z_2(1) = 1 \; , \; z_5(1) = \frac{\gamma_1(z_4(1) - 1)}{1 + \frac{4}{3}\,Rd} \; , \; z_7(1) = \gamma_2(z_6(1) - 1) \; , \; z_8(1) = 1,$$

$$z_2(\xi) \to 0 \; , \; z_4(\xi) \to 0 \; , \; z_6(\xi) \to 0 \; , \; z_8(\xi) \to 0 \qquad \text{when} \qquad \xi \to \infty.$$

3.5 Comparison and Discussion

Table 3.1: Numerical computations for skin friction coefficient when $m = 0.3$, $Pr = 10$, $n = 4$ $Q = 0.1$, $Sc = Sb = 0.3$, $\delta = \omega = 0.1$, $\sigma = 0.3$, $E = 0.1$, $Pe = Nt = 0.3$, $Nb = Rd = 0.4$, $\gamma_1 = 0.3$, $\gamma_2 = 0.4$

A	We	Gt	Gs	M	K_p	Carreau Fluid	Cross Fluid
-1.5	0.2	0.4	0.5	0.1	0.3	-2.12230	-1.82114
-2						-2.54336	-2.25594
-2.5						-2.99698	-2.70947
-1	0.1	0.4	0.5	0.1	0.3	-1.70643	-1.41847
	0.2					-1.74492	-1.41737
	0.3					-1.80245	-1.41256
-1	0.2	0.4	0.5	0.1	0.3	-1.74492	-1.41737
		0.6				-1.74431	-1.41676
		0.8				-1.74370	-1.41615
-1	0.2	0.4	0.5	0.1	0.3	-1.74492	-1.41737
			0.7			-1.68388	-1.35060
			0.9			-1.62389	-1.28463
-1	0.2	0.4	0.5	0.1	0.3	-1.74488	-1.41733
				0.5		-1.93698	-1.62305
				0.9		-2.11137	-1.80103
-1	0.2	0.4	0.5	0.1	0.3	-1.78650	-1.46492
					0.8	-2.01393	-1.70385
					1.3	-2.21935	-1.90856

For the considered problem, the results are plotted and tabulated as comparative analysis of Cross and Carreau fluid.

In Table 3.1 - 3.4, the comparison of local skin friction coefficient, local Nusselt number, local Sherwood number and density of motile micro-organisms has been noted down in response to varying parameters offering distinctive insight to the system's behaviour. Table 3.1 shows that,

Table 3.2: Computation of local Nusselt number when $We = 0.2$, $n = 4$, $Sc = 0.3$, $Sb = 0.3$, $\omega = 0.1$, $\sigma = 0.3$, $Pe = 0.3$, $Gt = 0.4$, $Gs = 0.5$, $\gamma_1 = 0.3$, $\gamma_2 = 0.4$, $\delta = 0.1$, $m = 0.3$, $K_p = 0.3$, $M = 0.1$, $E = 0.1$

A	Pr	Nt	Nb	Q	Rd	Carreau Fluid	Cross Fluid
-1.5	10	0.3	0.4	0.1	0.4	0.294531	0.294529
-2						0.295773	0.295772
-2.5						0.296562	0.296560
-1	6	0.3	0.4	0.1	0.4	0.288448	0.288456
	9					0.291607	0.291611
	12					0.293374	0.293377
-1	10	0.4	0.4	0.1	0.4	0.292348	0.292353
		0.6				0.292433	0.292438
		0.8				0.292511	0.292517
-1	10	0.3	0.5	0.1	0.4	0.292147	0.292151
			0.7			0.291820	0.291823
			0.9			0.291468	0.291473
-1	10	0.3	0.4	0.2	0.4	0.292228	0.292232
				0.6		0.291901	0.291906
				1.2		0.291303	0.291310
-1	10	0.3	0.4	0.1	0.4	0.292304	0.292308
					0.8	0.292648	0.292653
					1.2	0.292943	0.292950

in absolute sense higher drag force will be exerted during flow of Cross fluid other than Carreau fluid when varying the parameters like unsteadiness, flow index, temperature and concentration buoyancy, magnetic and porosity parameters. Simultaneously, it is observed that local skin friction is increasing function of A, M and K_p while, local skin friction coefficient is decreasing function of We, n, Gt and Gs.

In Table 3.2, it is found that Carreau fluids have slightly greater conductive heat transfer through the boundary when comparing with Cross fluids while increasing different parameters as tabulated for local Nusselt number computations. Table 3.3 depicts that Carreau fluids have little higher values of local Sherwood number than Cross fluid when altering the values of parameters such as A, Nt, Nb, Sc, σ, δ and m. Whereas, in case of rising activation parameter E, Cross fluid has uplifted rate of mass transfer of nanoparticles than Carreau fluid. In Table 3.4, it is noted that Cross fluids have enhanced local density of motile micro-organisms relative to flow of Carreau fluids.

The influence of unsteadiness parameter A on $g'(\xi)$ is depicted in Figure 3.2. Higher the unsteadiness in fluid flow while cylinder is stretching(expanding radially), lower will be the flow strength and their boundary layer thickness.

Figure 3.3 illustrates influence of Weissenberg number We on velocity field. Whenever relaxation time for Carreau fluid rises, it results growth in momentum boundary layer thickness and fluid

Table 3.3: Numerical computation of local Sherwood number when $We = 0.2$, $n = 4$, $Pr = 10$, $Q = 0.1$, $Sb = 0.3$, $\omega = 0.1$, $Pe = 0.3$, $Gt = 0.4$, $Gs = 0.5$, $\gamma_1 = 0.3$, $\gamma_2 = 0.4$, $Rd = 0.4$, $Kp = 0.3$, $M = 0.1$

A	Nt	Nb	Sc	σ	δ	m	E	Carreau Fluid	Cross Fluid
-1.5	0.3	0.4	0.2	0.3	0.1	0.3	0.1	0.262673	0.262616
-2								0.275247	0.275073
-2.5								0.285805	0.285561
-1	0.4	0.4	0.2	0.3	0.1	0.3	0.1	0.234231	0.234439
	0.6							0.209058	0.209325
	0.8							0.183853	0.184186
-1	0.3	0.5	0.2	0.3	0.1	0.3	0.1	0.254328	0.254474
		0.7						0.263028	0.263160
		0.9						0.267869	0.267993
-1	0.3	0.4	0.4	0.3	0.1	0.3	0.1	0.262039	0.262206
			0.6					0.285087	0.285202
			0.8					0.300551	0.300636
-1	0.3	0.4	0.2	0.3	0.1	0.3	0.1	0.245263	0.245473
				0.6				0.252601	0.252762
				1.2				0.264038	0.264143
-1	0.3	0.4	0.2	0.3	0.3	0.3	0.1	0.246201	0.246392
					0.7			0.246205	0.246396
					1.1			0.246209	0.246400
-1	0.3	0.4	0.2	0.3	0.1	0.3	0.1	0.245196	0.245408
						0.6		0.245197	0.245409
						0.9		0.245198	0.245410
-1	0.3	0.4	0.2	0.3	0.1	0.3	0.5	0.242512	0.242743
							1	0.240168	0.240417
							1.5	0.238677	0.238940

Table 3.4: Computation of local density of motile micro-organisms when $We = 0.2$, $n = 4$, $Pr = 10$, $Rd = Gt = 0.4$, $Gs = 0.5$, $Nt = \gamma_1 = 0.3$, $Gs = Nb = \gamma_2 = 0.4$, $Sc = \sigma = Kp = 0.3$, $Q = \delta = E = M = 0.1$, $m = 0.3$

A	Sb	Pe	ω	Carreau Fluid	Cross Fluid
-1.5	0.3	0.3	0.1	1.05739	1.05809
-2				1.23364	1.23595
-2.5				1.40993	1.41381
-1	0.3	0.3	0.1	0.769285	0.767227
	0.6			1.09263	1.08902
	0.9			1.39129	1.38647
-1	0.3	0.2	0.1	0.758444	0.756351
		0.6		0.802447	0.800494
		0.8		0.825087	0.823204
-1	0.3	0.3	0.2	0.771975	0.769930
			0.6	0.782734	0.780743
			1.2	0.798873	0.796962

strength. On contrary, increase in relaxation time for cross fluid shows little decline in momentum boundary layer.
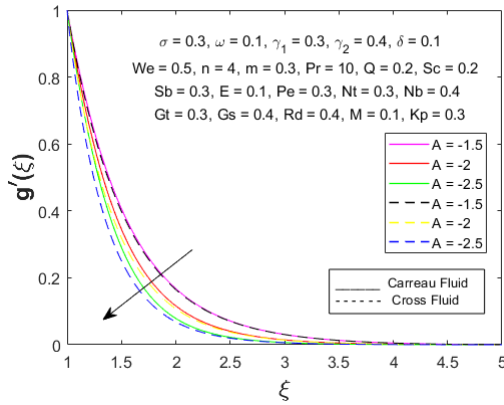

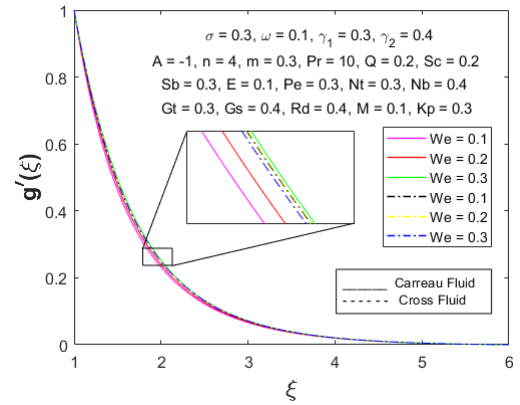Figure 3.2: Velocity field with changing unsteadiness parameter.

Figure 3.3: Velocity profile with varying Weissenberg number.

Figure 3.4 contributes in elaborating Lorentz force impact on velocity $g'(\xi)$ versus ξ graph in view of Cross and Carreau fluid. So, Lorentz force opposes near wall fluid in both cases, causing decrease in velocity profile. Momentum boundary layer thickness suppresses due to rising magnetic parameter for both fluids instead, thickness of boundary layer exhibited by Cross fluid is marginally varying to that of Carreau fluid when compared.
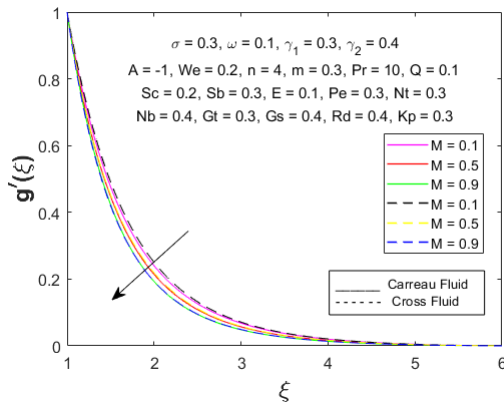

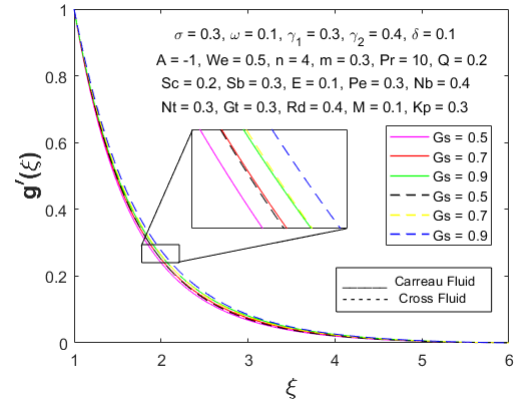Figure 3.4: Magnetic parameter via $g'(\xi)$.

Figure 3.5: Concentration buoyancy parameter via $g'(\xi)$.

The behavior of concentration buoyancy parameter Gs on $g'(\xi)$ is shown in Figure 3.5. Increment in velocity field happens due to higher concentration buoyancy parameter for Carreau as well as Cross fluid. Since, it is ratio of buoyancy force due to concentration gradients to the buoyancy force due to temperature gradients. Therefore, the buoyancy force dominates due to concentration gradient whenever concentration buoyancy parameter elevates.

In Figure 3.6, the influence of porosity parameter K_p on velocity profile $g'(\xi)$ is presented.
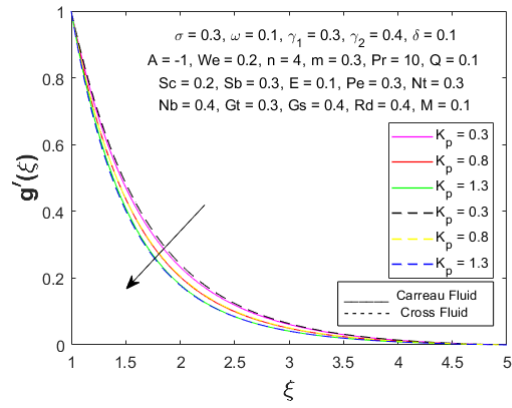
Figure 3.6: Effect of porosity parameter on velocity profile.

Physically, higher the percentage of void spaces or microstructures in the material causes slow movement of both fluids. Although, Cross fluids have smaller momentum boundary layer than Carreau fluids.

Chapter 4

Conclusion and Outlook

In view of unsteady, incompressible fluid flowing through porous medium that has been employed with two generalized Newtonian fluid models i-e Cross and Carreau viscosity models. These models are formulated under Brownian, thermophoresis and radiation effects over stretching cylinder.

So, the thesis comprises of computation and interpretation of two problems summarized in second and third chapter. Now, in order to conclude the problem elaborated in second chapter, we have enumerated the findings as,

- Rise in Weissenberg number We causes increase in fluid velocity.

- Due to increment in solutal Biot number and radiation parameter, local mass transfer of flow rises.

- Thermal Biot number and radiation parameter increments in local Nusselt number.

- Thermophoresis parameter Nt enhances and causes concentration of nanoparticles and boundary layer thickness to rise.

- Heat source Q and thermal conductivity parameter ϵ causes greater temperature profile and respective boundary layer.

The results found after modelling and computations of the problem presented in third chapter is as follows,

- Higher the unsteadiness in fluid flowing over stetching cylinder(expanding radially), there is diminished flow velocity.

- Increment in relaxation time causes considerable impact on movement of Carreau fluid flow irrespective to Cross fluid.

- The inclusion of the concentration buoyancy parameter has led to a more pronounced velocity profile for the Cross fluid model compared to the Carreau model.

- Carreau fluids have higher magnitude of drag force when interacted with fluid, relative to Cross fluids due to varying parameters such as unsteadiness parameter, Weissenberg number, temperature and concentration buoyancy parameters, magnetic and porosity parameter.

- Carreau fluids have greater local density of motile microorganisms than Cross fluids except for varying unsteadiness parameter.

Future Aspects

The future line of research after modelling problems involving stretching cylinder placed horizontally in a porous medium under magnetohydrodynamics, radiation, Brownian and thermophoresis effects are,

- The problem geometry may be assumed as rotating stretching cylinder.

- Geometry could be assumed as inclined stretching cylinder.

- Comparative analysis of the considered generalized Newtonian fluid models with other non-Newtonian fluid models.

- Extensive comparative analysis utilizing numerical simulations for three dimensional geometry instead of two dimensional.

Bibliography

[1] Altan, T., S. Oh, and H. Gegel. "Metal forming fundamentals and applications Metals park." OH: American Society of Metals (1979).

[2] Fisher, E. G. "Extrusion of Plastics, Wiley, New York, 1976."

[3] Tadmor, Zehev, and Imrich Klein. Engineering principles of plasticating extrusion. New York: Van Nostrand Reinhold Company, 1970.

[4] Wang, Ch Y. "Fluid flow due to a stretching cylinder." The Physics of fluids 31, no. 3 (1988): 466-468.

[5] Imtiaz, Maria, Tasawar Hayat, and Ahmed Alsaedi. "Mixed convection flow of Casson nanofluid over a stretching cylinder with convective boundary conditions." Advanced Powder Technology 27, no. 5 (2016): 2245-2256.

[6] Pandey, Alok Kumar, and Manoj Kumar. "Boundary layer flow and heat transfer analysis on Cu-water nanofluid flow over a stretching cylinder with slip." Alexandria Engineering Journal 56, no. 4 (2017): 671-677.

[7] Poply, V., P. Singh, and A. K. Yadav. "Analysis of stability and dual solution of MHD outer fluid velocity with partial slip on a stretching cylinder. 10." Int. J. Adv. Trends Comput. Appl.(IJATCA) 1 (2019): 194-203.

[8] Ali, Azhar, Dil Nawaz Khan Marwat, and Saleem Asghar. "Viscous flow over a stretching (shrinking) and porous cylinder of non-uniform radius." Advances in Mechanical Engineering 11, no. 9 (2019): 1687814019879842.

[9] Sohail, Muhammad, and Rahila Naz. "Modified heat and mass transmission models in the magnetohydrodynamic flow of Sutterby nanofluid in stretching cylinder." Physica A: Statistical Mechanics and its Applications 549 (2020): 124088.

[10] Iqbal, W., and M. Jalil. "Numerical analysis for the effects of boundary layer flow over an exponentially stretching cylinder embedded in a porous medium moving with nonlinear velocity." AIP Advances 11, no. 12 (2021): 125322.

[11] Umeshaiah, Mahadevaiah, JavaliK Madhukesh, Umair Khan, Saurabh Rana, Aurang Zaib, Zehba Raizah, and Ahmed M. Galal. "Dusty Nanoliquid Flow through a Stretching Cylinder in a Porous Medium with the Influence of the Melting Effect." Processes 10, no. 6 (2022): 1065.

[12] Pearson, J. R. A., and P. M. J. Tardy. "Models for flow of non-Newtonian and complex fluids through porous media." Journal of Non-Newtonian Fluid Mechanics 102, no. 2 (2002): 447-473.

[13] Cross, Malcolm M. "Rheology of non-Newtonian fluids: a new flow equation for pseudo-plastic systems." Journal of colloid science 20, no. 5 (1965): 417-437.

[14] Barnes, Howard A., John Fletcher Hutton, and Kenneth Walters. An introduction to rheology. Vol. 3. Elsevier, 1989.

[15] Escudier, M. P., I. W. Gouldson, A. S. Pereira, F. T. Pinho, and R. J. Poole. "On the reproducibility of the rheology of shear-thinning liquids." Journal of Non-Newtonian Fluid Mechanics 97, no. 2-3 (2001): 99-124.

[16] Khan, Masood, Mehwish Manzur, and Masood ur Rahman. "On axisymmetric flow and heat transfer of Cross fluid over a radially stretching sheet." Results in physics 7 (2017): 3767-3772.

[17] Nayak, Manoj Kumar, Vinay Shankar Pandey, Dharmendra Tripathi, Noreen Sher Akbar, and Oluwole D. Makinde. "3D MHD cross flow over an exponential stretching porous surface." Heat Transfer 49, no. 3 (2020): 1256-1280.

[18] Hina, Sadia, Ayesha Shafique, and M. Mustafa. "Numerical simulations of heat transfer around a circular cylinder immersed in a shear-thinning fluid obeying Cross model." Physica A: Statistical Mechanics and its Applications 540 (2020): 123184.

[19] Carreau, Pierre J. "Rheological equations from molecular network theories." Transactions of the Society of Rheology 16, no. 1 (1972): 99-127.

[20] Sochi, Taha. "Analytical solutions for the flow of Carreau and Cross fluids in circular pipes and thin slits." Rheologica Acta 54 (2015): 745-756.

[21] Choi, S. US, and Jeffrey A. Eastman. Enhancing thermal conductivity of fluids with nanoparticles. No. ANL/MSD/CP-84938; CONF-951135-29. Argonne National Lab.(ANL), Argonne, IL (United States), 1995.

[22] Kuznetsov, Andrey V. "Nanofluid bioconvection in water-based suspensions containing nanoparticles and oxytactic microorganisms: oscillatory instability." Nanoscale research letters 6, no. 1 (2011): 1-13.

[23] Buongiorno, Jacopo. "Convective transport in nanofluids." (2006): 240-250.

[24] Wakif, Abderrahim, Ali Chamkha, I. L. Animasaun, M. Zaydan, Hassan Waqas, and R. Sehaqui. "Novel physical insights into the thermodynamic irreversibilities within dissipative EMHD fluid flows past over a moving horizontal riga plate in the coexistence of wall suction and joule heating effects: a comprehensive numerical investigation." Arabian Journal for Science and Engineering 45, no. 11 (2020): 9423-9438.

[25] Alshehri, Nawal A., Awatef Abidi, Muhammad Riaz Khan, Yanala Dharmendar Reddy, Saim Rasheed, Elham Alali, and Ahmed M. Galal. "Unsteady convective MHD flow and heat transfer of a viscous nanofluid across a porous stretching/shrinking surface: existence of multiple solutions." Crystals 11, no. 11 (2021): 1359.

[26] Katagiri, Masakazu. "On the separation of magnetohydrodynamic flow near the rear stagnation point." Journal of the Physical Society of Japan 27, no. 4 (1969): 1045-1050.

[27] Hayat, Tasawar, Muhammad Tamoor, Muhammad Ijaz Khan, and Ahmad Alsaedi. "Numerical simulation for nonlinear radiative flow by convective cylinder." Results in physics 6 (2016): 1031-1035.

[28] Mishra, Ashish, and Manoj Kumar. "Velocity and thermal slip effects on MHD nanofluid flow past a stretching cylinder with viscous dissipation and Joule heating." SN Applied Sciences 2, no. 8 (2020): 1-13.

[29] Tayebi, Tahar, and Ali J. Chamkha. "Entropy generation analysis due to MHD natural convection flow in a cavity occupied with hybrid nanofluid and equipped with a conducting hollow cylinder." Journal of Thermal analysis and Calorimetry 139, no. 3 (2020): 2165-2179.

[30] Khan, M. Ijaz, Sumaira Qayyum, S. Kadry, W. A. Khan, and S. Z. Abbas. "Irreversibility analysis and heat transport in squeezing nanoliquid flow of non-Newtonian (second-grade) fluid between infinite plates with activation energy." Arabian Journal for Science and Engineering 45, no. 6 (2020): 4939-4947.

[31] Zhao, Tie-Hong, M. Ijaz Khan, and Yu-Ming Chu. "Artificial neural networking (ANN) analysis for heat and entropy generation in flow of non-Newtonian fluid between two rotating disks." Mathematical Methods in the Applied Sciences (2021).

[32] Nazeer, Mubbashar, Farooq Hussain, M. Ijaz Khan, Essam Roshdy El-Zahar, Yu-Ming Chu, and M. Y. Malik. "Theoretical study of MHD electro-osmotically flow of third-grade fluid in micro channel." Applied Mathematics and Computation 420 (2022): 126868.

[33] Arrhenius, Svante. "On the heat of dissociation and the influence of temperature on the degree of dissociation of the electrolytes." Journal of Physical Chemistry 4, no. 1 (1889): 96-116.

[34] Irfan, M., W. A. Khan, M. Khan, and M. Mudassar Gulzar. "Influence of Arrhenius activation energy in chemically reactive radiative flow of 3D Carreau nanofluid with nonlinear mixed convection." Journal of Physics and Chemistry of Solids 125 (2019): 141-152.

[35] Khan, Arshad, Anwar Saeed, Asifa Tassaddiq, Taza Gul, Safyan Mukhtar, Poom Kumam, Ishtiaq Ali, and Wiyada Kumam. "Bio-convective micropolar nanofluid flow over thin moving needle subject to Arrhenius activation energy, viscous dissipation and binary chemical reaction." Case Studies in Thermal Engineering 25 (2021): 100989.

[36] Aziz, Abdul. "A similarity solution for laminar thermal boundary layer over a flat plate with a convective surface boundary condition." Communications in Nonlinear Science and Numerical Simulation 14, no. 4 (2009): 1064-1068.

[37] Makinde, Oluwole D., and A. Aziz. "Boundary layer flow of a nanofluid past a stretching sheet with a convective boundary condition." International Journal of Thermal Sciences 50, no. 7 (2011): 1326-1332.

[38] Ray, Atul Kumar, B. Vasu, P. V. S. N. Murthy, and Rama SR Gorla. "Non-similar solution of Eyring–Powell fluid flow and heat transfer with convective boundary condition: Homotopy Analysis Method." International Journal of Applied and Computational Mathematics 6, no. 1 (2020): 1-22.

[39] Babu, Dondu Harish, Nainaru Tarakaramu, Panyam Venkata Satya Narayana, Ganganapalli Sarojamma, and Oluwole Daniel Makinde. "MHD flow and heat transfer of a Jeffrey fluid over a porous stretching/shrinking sheet with a convective boundary condition." Int. J. Heat Technol 39, no. 3 (2021): 885-894.

[40] Mabood, F., H. Berrehal, T. A. Yusuf, and W. A. Khan. "Carbon nanotubes-water between stretchable rotating disks with convective boundary conditions: Darcy-Forchheimer scheme." International Journal of Ambient Energy 43, no. 1 (2022): 3981-3994.

[41] Shampine, Lawrence F., Jacek Kierzenka, and Mark W. Reichelt. "Solving boundary value problems for ordinary differential equations in MATLAB with bvp4c." Tutorial notes 2000 (2000): 1-27.

[42] Fang, Tie-Gang, Ji Zhang, Yong-Fang Zhong, and Hua Tao. "Unsteady viscous flow over an expanding stretching cylinder." Chinese Physics Letters 28, no. 12 (2011): 124707.

[43] Khan, Masood, Muhammad Azam, and A. S. Alshomrani. "On unsteady heat and mass transfer in Carreau nanofluid flow over expanding or contracting cylinder with convective surface conditions." Journal of Molecular Liquids 231 (2017): 474-484.

[44] Azam, M., T. Xu, and M. Khan. "Numerical simulation for variable thermal properties and heat source/sink in flow of Cross nanofluid over a moving cylinder." International Communications in Heat and Mass Transfer 118 (2020): 104832.

[45] Arunachalam, M., and N. R. Rajappa. "Thermal boundary layer in liquid metals with variable thermal conductivity." Flow, Turbulence and Combustion 34, no. 2 (1978): 179-187.